Photonuclear reactions with charged particles detection for nuclear astrophysics studies

C.R. Brune[1], C. Matei[2*], S.D Pain[3] and R. Smith[4†]

[1]Ohio University, Athens, 45701, Ohio, USA.
[2*]Extreme Light Infrastructure - Nuclear Physics, Horia Hulubei National Institute for R&D in Physics and Nuclear Engineering, Bucharest-Magurele, 077125, Romania.
[3]Oak Ridge National Laboratory, Oak Ridge, 37831, Tennessee, USA.
[4]Department of Engineering and Mathematics, Sheffield Hallam University, Sheffield, S1 1WB, UK.

*Corresponding author(s). E-mail(s): Catalin.Matei@eli-np.ro;
†These authors contributed equally to this work.

Abstract

Measurements of $(\boldsymbol{\gamma}, \boldsymbol{p})$ and $(\boldsymbol{\gamma}, \boldsymbol{\alpha})$ photonuclear reaction cross sections are relevant for several nucleosynthesis scenarios, from the primordial Big Bang, to stellar burning, and the p-process. Studies of photonuclear reaction cross sections marked a steady development in the last 20 years with the advent of mono-energetic $\boldsymbol{\gamma}$-ray beam facilities and improved detection methods. Charged-particle detection from photon-induced reactions in solid targets is mainly achieved with silicon-strip detectors, while time projection chambers were developed for measurements with active gas targets. This review tracks the evolution of charged-particle detection methods and highlights recent $^{\mathbf{7}}\mathrm{Li}(\boldsymbol{\gamma}, \boldsymbol{t})^{\mathbf{4}}\mathrm{He}$ and $^{\mathbf{16}}\mathrm{O}(\boldsymbol{\gamma}, \boldsymbol{\alpha})^{\mathbf{12}}\mathrm{C}$ cross section measurements using mono-energetic $\boldsymbol{\gamma}$-ray beams.

1 Introduction

Radiative capture processes such as (p,γ), (α,γ), and (n,γ) have implications in a wide range of astrophysical scenarios, from Big Bang nucleosynthesis to

helium burning and the final burning stages of a massive star's existence, to the p-process nucleosynthesis. Studying the inverse, photon-induced reactions, has been recognized since the 1950's as a viable method for investigating some of the puzzles in nuclear physics and astrophysics. The early work on photon-induced reactions was reviewed by Strauch in 1953 [1], who defined the term "photonuclear reactions" as "any photon initiated nuclear transformation in which either one or many γ-rays, neutrons, protons, or aggregates of nucleons are emitted". More recent and comprehensive reviews of the entire photonuclear field are given by Zilges *et al.* [2] in 2022, Howell *et al.* [3] in 2021, and Weller *et al.* [4] in 2009.

The principle of detailed balance based on the notion of invariance under time reversal allows the calculation of the cross section $\sigma_{capture}$ for the capture A(x,γ)B processes to the ground state of nucleus B by measuring the cross section σ_γ for the inverse, photo-disintegration B(γ,x)A reaction [5]:

$$\sigma_{capture} = \frac{2(2j_B+1)k_\gamma^2}{(2j_A+1)(2j_x+1)k_x^2}\sigma_\gamma, \tag{1}$$

where x is the captured particle, j are the ground state spins, k_x^2 and k_γ^2 are the wave numbers for capture and photo-disintegration, respectively ($k_x^2 = 2\mu_{Ax}E_x\hbar^{-2}$, $k_\gamma^2 = E_\gamma^2\hbar^{-2}c^{-2}$).

The experimental photo-disintegration cross section for thin targets is given by:

$$\sigma_(\gamma,r)(E_\gamma) = \frac{N_r(E_\gamma)}{N_t\epsilon_r\Phi(E_\gamma)}, \tag{2}$$

where $N_r(E_\gamma)$ is the number of detected reaction products, N_t the number of target nuclei per unit area, ϵ_r the detection efficiency including the probability for the reaction products to be absorbed in the target and the solid angle correction, and $\Phi(E_\gamma)$ is the integrated γ-ray beam intensity.

Experimentally, measurements of the photo-disintegration process can offer some advantages over the radiative capture process. Applying the principle of detailed balance to two of the reactions discussed in this review, the radiative α-capture on ^{12}C and on ^{3}H, results in gains between 50 and 60 for the photo-disintegration cross section. This increase in cross section amounts to a considerable advantage in view of the low cross sections responsible for many nucleosynthesis processes. Another advantage of measurements with gamma beams is that the incident beam does not experience electronic energy loss as it passes through the target material.

Radiative capture reaction rates are defined in many cases by a combination of ground state and excited states contributions in the final nucleus. A measurement of a photo-disintegration reaction cross section, where the target nucleus is always in the ground state, only yields directly the cross section for the time-reversed process of radiative capture into the ground state. Photo-disintegration measurements are thus most useful for constraining the astrophysical rate if the ground state contribution is larger than the contribution from the excited states.

Measurements of photon-induced reaction cross sections with emission and detection of charged particles were reported since the 1970's. While the detection of photon scattering, neutron emission, or activation is simplified by the long range of the detected radiations, charged-particles detection requires the use of targets and detectors inside a vacuum chamber or the use of an active target. Detection of the reaction products from the photo-disintegration mainly of lighter nuclei started at bremsstrahlung facilities using solid targets and surface barrier silicon detectors in late 70's [6], with several early experiments presented in Section 2.1. Time projection chambers, conventional instruments in experimental nuclear physics, have been used for photo-disintegration measurements with gaseous targets since early 2000's [7, 8]. These early experiments together with the development of an optical TPC (O-TPC) for the study of the $^{16}O(\gamma,\alpha)^{12}C$ reaction are described in Sections 3.1-3.3.

A proof-of-principle experiment using a bubble chamber for measuring the $^{15}N(\alpha,\gamma)^{19}F$ through the inverse $^{19}F(\gamma,\alpha)^{15}N$ was reported by Ugalde et al [9] in 2013 in an experiment at the High Intensity γ-ray Source (HIγS). The technique makes use of a superheated liquid to produce visible bubbles when a charged particle deposits energy in the liquid target. The detector was deemed insensitive to the γ-ray beam at a level of one part in 10^9. No further uses of the method or new devices were reported since 2013. However, a detector based on related concepts has been developed for neutron detection [10].

In the past four decades, photon sources have steadily advanced, from neutron and particle induced γ-ray emission from various nuclei, to bremsstrahlung and present-day tunable, mono-energetic γ-ray facilities. Since the early 2000s, the High Intensity γ-ray Source (HIγS) operated by the Triangle Universities National Laboratory (TUNL) has been the world-leading γ-ray beam facility, producing an intense (10^3 photons/s/eV), quasi mono-energetic (bandwidth of 3-5%), maximum energy of 120 MeV, highly polarized γ-ray source dedicated to low- and medium-energy nuclear physics research [4]. The γ-ray beams are produced via the laser Compton backscattering process which involves colliding photons generated by a free-electron laser with high-energy electrons in a storage ring.

The Variable Energy Gamma (VEGA) System, which in under implementation at Extreme Light Infrastructure - Nuclear Physics (ELI-NP) in Romania, uses a storage ring for an Inverse Compton Scattering (ICS) source. The storage ring is filled by a warm linear accelerator with a maximum energy of 800 MeV. A laser system drives a high-finesse optical cavity to resonantly build-up pulsed laser power. Mono-energetic photon beams are produced via laser Compton backscattering of laser pulses off the relativistic electron beam in the storage ring. The high-brilliance narrow-bandwidth γ-ray beam will be delivered with energies up to 19.5 MeV, a spectral density higher than 5×10^3 photons/s/eV, bandwidth of 0.5%, and linear polarization higher than 95% [11]. The nuclear astrophysics program with VEGA at ELI-NP includes studies of (γ,p) and (γ,α) photo-disintegration reactions on light nuclei for Big

Bang nucleosynthesis (^{2}H, $^{6-7}$Li), heavier nuclei for stellar burning (^{16}O, ^{19}F, ^{22}Ne, ^{24}Mg) and p-process (^{74}Se, ^{78}Kr, ^{84}Sr, ^{92}Mo, ^{96}Ru) [12–14].

In this paper we review the development and look at the future of photonuclear reactions with charged particle detection from solid and gas targets by highlighting the main detection instruments and several reactions relevant to nuclear astrophysics.

2 Measurements of charged particles from solid targets

An overview of photonuclear experiments before 2010 with detection of charged particles is given in the beginning of this section, while a recent ^{7}Li$(\gamma,t)^{4}$He experiment is described in Section 2.3. A review of the evolution of silicon-detector arrays over the last 20 years in Section 2.2 sets the stage for challenges and future in the field of photon-induced measurements with detection of charged particles from solid targets.

2.1 Previous photon-induced measurements with solid targets

Very few photon-induced cross section measurements with detection of charged particles, relevant to nuclear astrophysics, were reported in the last 50 years. Experiments were carried out since the late 70's to study the photo-disintegration mainly of lighter nuclei by using bremsstrahlung photons or neutron induced γ-ray emission and various types of surface barrier silicon detectors.

Junghans *et al.* [6] reported results in 1979 from the photo-disintegration of both ^{6}Li and ^{7}Li using a bremsstrahlung beam from the University of Giessen 65 MeV LINAC. Isotopically enriched lithium metal targets were rolled into a thickness of 1.5 mg/cm^2. Measurements were performed with endpoint energies up to 35 MeV for ^{6}Li and 50 MeV for ^{7}Li. The excitation function was determined using two-body kinematics from the measured triton and α-particle energy. The uncertainties in the data were large as the thresholds in the ΔE silicon telescopes used for detecting the tritons and α-particles were 1.7 MeV and 5 MeV respectively. No systematic uncertainties were listed for the ^{7}Li$(\gamma,t)^{4}$He reaction cross section from Ref. [6], although a 15% uncertainty was reported for the ^{6}Li$(\gamma,t)^{3}$He reaction measured during the same experiment.

Bremsstrahlung beams with an end-point energy of 14 MeV, generated by the MAinz-MIcrotron (MAMI), was used by Zieger *et al.* to study the differential cross section of the ^{2}H(γ,p)n reaction [15]. The target consisted of a stack of two pieces of deuterated polyethylene (23.7% concentration of ^{2}H) foils with a total thickness of 9.76 mg/cm^2. The protons were magnetically deflected from the photon beam and focused on a surface barrier detector. The surface barrier detector was a circular, partially depleted detector with a depletion depth of about 300 μm allowing the detection of protons with

energies up to 6 MeV. The ^{2}H(γ,p)n differential cross section was determined at 10.74 MeV photon energy averaged over a 4.6 MeV range. The results from these measurements were published in 1986.

Another photo-disintegration measurement on the ^{7}Li isotope was reported by Likhachev *et al.* [16] in 2005 with monochromatic photons from neutron capture reactions at the IPEN/CNEN-SP IEA-R1 research reactor in Brazil. The incident photon spectrum available with the selected targets was between 6.4 to 6.7 MeV and 8.5 to 9 MeV. Metallic natural lithium foils of 50 and 100 μm were placed inside a vacuum chamber. Only tritons were detected in seven silicon strip detectors covering angles between 30 and 150°. The α-particles lost significant energy in the target and could not be separated from background. The uncertainties in the data were probably larger then those reported in the measurement of Ref. [6] as no α-particles were detected and the tritons were also produced by the ^{6}Li(n,t)^{4}He reaction. No systematic uncertainties were listed for the $^{7}\mathrm{Li}(\gamma, t)^{4}\mathrm{He}$ reaction cross section from Likhachev *et al.* [16] but a good agreement was reported with results of Junghans *et al.* [6] in the overlapping energy range.

2.2 Evolution and status of silicon detector arrays

Since the 1980s, the availability of large-area ion-implanted silicon detectors [17], which can be fabricated with near-arbitrary segmentation, have enabled the construction of large-solid-angle arrays with high segmentation. Such large-area detectors are critical to achieve the high detection efficiency needed for experiments with relatively weak beam intensities ($< 10^{6-7}$), common to both radioactive ion beams and gamma beams. The segmentation is necessary for experiments with strong kinematic shifts, the correlation and kinematic reconstruction of reactions with multiple particles in the exit channel, and to reduce the amplitude of electron-induced signals on a per channel basis (a common issue due to the beta decay of radioactive beams, and Compton-scattered electrons from gamma beams).

The Louvain-Edinburgh Detector Array (LEDA) [18] was one of the first arrays of highly-segmented large-area silicon detectors, built around custom-designed model YY1 detectors from Micron Semiconductor Ltd (MSL), and custom front-end electronics. These 8-fold annular detectors, which are segmented to provide polar angle in 16 strips with 5-mm pitch, taking advantage of the azimuthal symmetry of two-body reactions, have subsequently been adopted in other arrays deployed in both planar and tilted configurations, such as SIDAR [19], YLSA [20], TUDA [21] and TECSA [22]. More recently, tilted arrays have been developed of MSL MMM detectors, such as CAKE [23] and SABRE [24]. These MMM detectors have a larger active area and slightly larger strip pitch (6.4 mm) than YY1 detectors, but also have 8-fold segmentation on the n-type face of the detectors, providing almost and order-of-magnitude improvement in azimuthal angular resolution. These detectors are available with thin entrance windows, making them well suited to the

measurement of low-energy particles, such as particle decay channels following transfer reactions.

Such annular arrays are inherently well-suited to measure at the most forward and backward angles with respect to the beam axis. To achieve 4π coverage, a different geometry of detector is needed to cover the angles closer to 90 degrees. A neutral geometry for this angular range is a barrel type configuration, with detectors arranged in one or more rings around the beam axis. A special case of this is a four-sided box configuration, which can provide high solid-angle coverage at the expense of limited target-detector distance. This has the advantage of being compact enough for operation within the tight confines of other detectors (such as γ-ray detectors arrays), but comes at the expense of increased contributions of the finite beam-spot size to the angular uncertainty in kinematic reconstructions.

The cost of such 4π large-solid angle arrays is electronics channel count which, depending on the degree of segmentation required, can range between hundreds or thousands of channels. Over the last two decades or so, two approaches have been taken to address this problem.

The first approach is via large-area resistive strip detectors, which have opened the possibility of near-4π silicon detector arrays with manageable channel counts (hundreds) while maintaining the good ($\sim$1 mm) position resolution to be matched to the beam optics of tandem and LINAC facilities. In this manner, mm-position resolution can be obtained over the length of a strip of many centimeters in total length using just two electronics channels, leading to a channel saving of 1-2 orders of magnitude compared to mm-pitch segmentation across this length. The position resolution aids with the reconstruction of reactions with large kinematic shifts, and the kinematic correlation between multiple particles, though does not help with the limitation of electron-induced signals.

The Oak Ridge Rutgers University Barrel Array (ORRUBA) [25] is a quasi-4π array of silicon detectors with about 1 degree resolution in polar angle. It was initially designed around a barrel configuration of resistive-strip detectors, oriented symmetrically around the target co-axially with the beam direction, optimized for measurements with tandem-quality beams. Two rings of detectors, each of 12 X3 model detectors from Micron Semiconductor Ltd (MSL). These detectors have an active area of 75 x 40 mm, and are divided into four 10-mm wide resistive strips running along the 75-mm length. They are available in thicknesses up to 1000 um, sufficient to stop protons of almost 12 MeV. For particle identification, transmission detectors can be added to form charged-particle telescopes, using BB10 detectors from MSL. These are the same active area as X3 detectors, but divided into 8 non-resistive strips and are typically 65 μm thick. The double-ringed barrel covers approximately 45 to 135 degrees, with 70-80% azimuthal coverage. More recently, the X3 detectors have been replaced with sX3 detectors, which are identical except for 4-way segmentation on the n-type contact of the detector. This level of segmentation reduces the

capacitance per n-type contact by a factor of four, leading to improved resolution by a comparable factor, with high-resolution signals not subject to the ballistic deficit issues typically associated with readout of the resistive strips. The barrel amounts to 144 channels per ring of position sensitive detectors, or 480 channels for two rings of telescopes.

The forward and backward regions not subtended by the barrel were initially covered by arrays of YY1 detectors, such as in Fig. 1. More recently, to facilitate more compact setups that fit within large germanium γ-ray detector arrays (see Section 2.4), Gammasphere and GRETINA, custom endcaps of quadrant-style annular detectors, model QQQ5 from MSL, have been adopted. Each quadrant is segmented into 32 annular strips on the junction face of the detector, with a thin ($\sim$100 nm) entrance window for minimal dead-layer effects on low-energy particles. The n-type face is divided into four radial contacts, providing $\sim$12 deg resolution in azimuthal angle. These detectors are designed with minimal frames and inbuilt flat-flex cables to maximize solid-angle coverage, and can be stacked in telescopes of arbitrary numbers of layers.

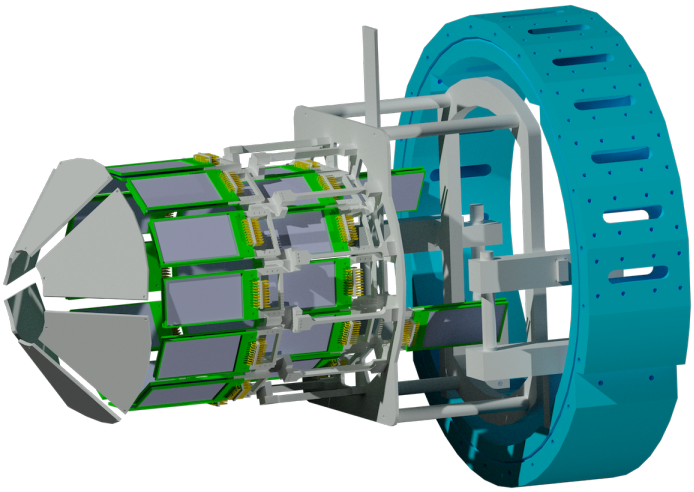

Fig. 1 CAD model of ORRUBA, with two rings of telescopes, comprised of BB10 and sX3 detectors, and a single endcap comprised of a lampshade arrangement of YY1 detectors (far left of image). All signals are brought out to the preamplifier mounting ring at the far right, from which the array is mechanically supported.

ELISSA (ELI Silicon Strip Array) is a silicon detector array developed at ELI-NP for nuclear astrophysics studies using γ-ray beams. The array consists of 35 X3 position-sensitive silicon-strip detectors (1000 μm) arranged into a three-ring barrel configuration [12, 26]. The angular coverage is extended by using two assemblies of four QQQ3 segmented end-cap detectors (300 and 500 μm).

The second approach to achieve a high-solid angle quasi-4π array with sufficient angular resolution is to highly segment the barrel detectors. Instrumenting arrays with such large channel counts with conventional electronics is cost-prohibitive. Instead, Application-Specific Integrated Circuits (ASICs) have been developed to achieve cost effective high-density electronics for large-channel-count arrays. The HINP-16 ASICs [27] have been developed at Washington University initially for use instrumenting the High Resolution Array (HIRA) [28], a $\sim$2000 channel array of twenty charged-particle telescopes backed by CsI detectors aimed at reactions using in-flight RIBs at intermediate energies. The HINP-16 ASICs are based around a 16-channel integrated circuit that incorporates charge-sensitive preamplifiers, shaping and peak sampling, timing and discriminator circuits, ultimately providing multiplexed signals to an off-chip pipelined ADC.

The superORRUBA array [29] utilizes custom-designed BB15 detectors from MSL, instrumented using the HINP-16 ASICs. These detectors have the same active area and mounting footprint as the X3/sX3 detectors, but instead of employing position-sensitive strips using resistive charge division, the 75-mm length of the detector is divided into 64 $\sim$1.3 mm strips. The n-type face of the detector is divided into four 10-mm wide contacts to maintain the same azimuthal resolution of an X3/sX3 detector. This approach provides sufficient position resolution that does not rely on resistive strips, with their associated position-dependent energy thresholds and ballistic deficit issues (non-linear energy response due to position-dependent signal risetime variations), but at the expense of 68 vs 12 channels per detector. A complete ring of BB15 detectors requires 816 electronics channels, as opposed to 144 channels for the equivalent ring of X3 detectors. A full two-ring array of BB15 telescopes totals 1820 channels. Though originally developed for experiments at the Holifield Radioactive Ion Beam Facility, superORRUBA has more recently been employed as the detector for the JENSA supersonic gas-jet target [30, 31] at the ReA3 Facility at the National Superconducting Cyclotron Laboratory, now the Facility for Rare Isotope Beams (FRIB), for measurements of (α,p) reactions for nuclear astrophysics.

2.3 Recent ^{7}Li$(\gamma, t)^{4}$He measurement at HIγS

The ^{7}Li$(\gamma, t)^{4}$He ground-state cross section was recently measured at High Intensity γ-ray Source (HIγS) between $E_\gamma = 4.4$ and 10 MeV [32]. This experiment marks the first time a large-area silicon-strip detector array was used for detecting charged particles from a photo-disintegration reaction induced by a mono-energetic γ-ray beam.

The ^{7}Li$(\gamma,t)^{4}$He measurement is relevant for solving the disagreement between the experimental and theoretical capture cross section in the mirror α-capture reactions ^{3}H$(\alpha,\gamma)^{7}$Li and ^{3}He$(\alpha,\gamma)^{7}$Be. While for ^{3}He$(\alpha,\gamma)^{7}$Be the theoretical calculations are in agreement with recent measurements [33, 34], there is a 15-20% difference [35, 36] between the calculated capture cross section for the mirror ^{3}H$(\alpha,\gamma)^{7}$Li reaction and the experimental data of Brune *et al.* [37].

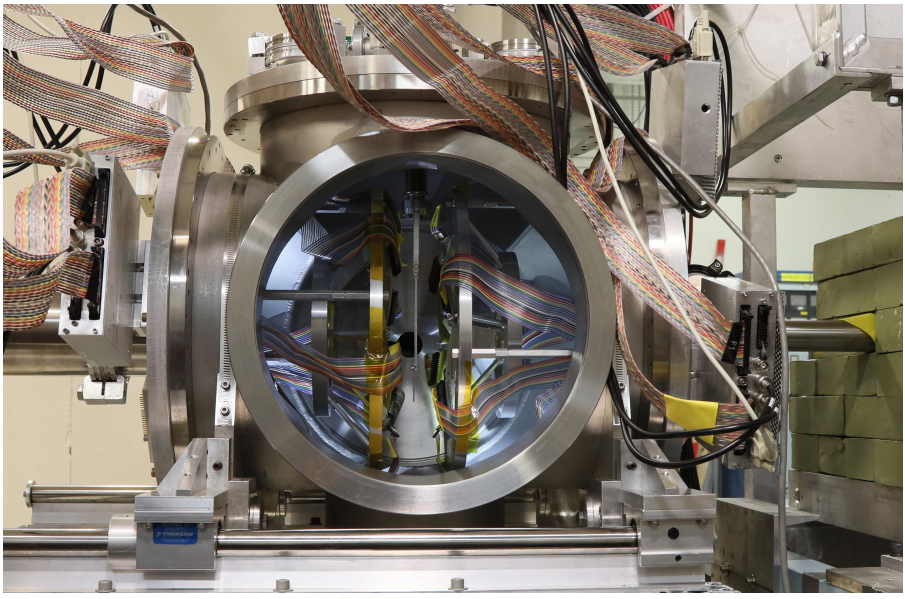

Fig. 2 Photo of the setup for the ^{7}Li$(\gamma,t)^{4}$He measurement at HIγS. The vacuum chamber contains two lampshade configurations of YY1 detectors of the SIDAR array, symmetrically mounted upstream and downstream of the target. Beam enters from the right, via an extended pipe upstream with an entrance window to the vacuum system, shielded from the setup by a lead castle.

The photo-disintegration of ^{7}Li generated back-to-back tritons and α particles which were detected in the SIDAR array of segmented silicon-strip detectors. Thin targets of natural LiF (300 and 600 μg/cm^{2}), evaporated onto 1.3 μm-thick mylar backing, were used to enable both the α and triton to escape the target and be detected. SIDAR was assembled in a lampshade configuration with 12 YY1 detectors of 300, 500, and 1000 μm thickness distributed between two hemispheres, mounted in the ORRUBA vacuum chamber as shown in Fig. 2. A thin (1.25-inch diameter) entrance window was used, mounted onto the end of a pipe $\sim$1.5 m upstream of the target, and shielded by a lead castle. The choice of detector thicknesses was constrained by SIDAR detector-pool availability, but also enabled a determination of the magnitude of beam-induced backgrounds in different thicknesses of silicon detector. This symmetrical detector arrangement enabled back-to-back detection of the α and

triton ejectiles, enabling energy, angle and timing cuts to be placed on the two correlated particles. Such coincidence requirements aid substantially in separating signals of interest from beam-induced electron backgrounds, with a 1-2 orders of magnitude reduction in the electron-induced backgrounds, as in Fig. 3.

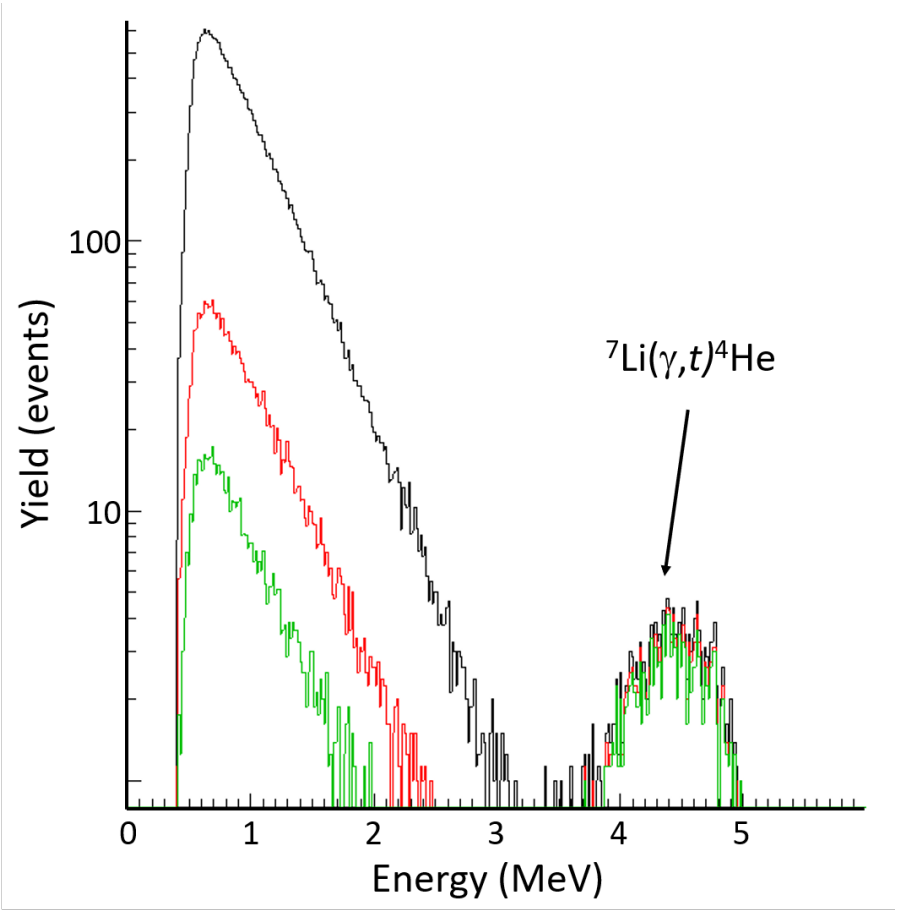

Fig. 3 Summed energy spectrum from SIDAR detectors from the $^7\mathrm{Li}(\gamma,t)^4\mathrm{He}$ experiment, with no geometric conditions (black), with a back-to-back detector coincidence (red) and a back-to-back strip coincidence (green). These spatial cuts suppress the uncorrelated electron backgrounds, with negligible loss of the genuinely coincident ejectiles from $^7\mathrm{Li}(\gamma,t)^4\mathrm{He}$ events.

The $^7\mathrm{Li}(\gamma,t)^4\mathrm{He}$ ground state cross section was calculated using the number of ^{7}Li nuclei per unit area in the LiF layer, the number of detected α-triton coincidences corrected for the detection efficiency, and the integrated γ-ray beam intensity as described by Eq. 2. While α-triton coincidences were clearly

identified in all detectors for γ-ray beam energies above 6 MeV, at lower energies they can only be separated from the beam-induced background in the 300 μm detectors (selection procedures described in detail in [32]). The beam-induced background recorded by the silicon detectors originates from Compton scattering in materials in, around, and upstream from the vacuum chamber. The γ-ray beam intensity was primarily determined by activation of ^{197}Au foils [38, 39] at 9 and 10 MeV and scaled at lower energies from relative measurements using the d(γ,n)p reaction and a thin plastic scintillator (details on activation and d(γ,n)p measurements in [32]). There was very good agreement between the γ-ray beam intensity determined by these methods and the values reported from the HIγS accelerator parameters. The main sources of systematic uncertainties for the calculated ground state cross section were the target thickness and homogeneity estimated at 10%, the selection procedure for the coincidences between 5% (above 6 MeV) and 10% (below 6 MeV), the solid angle correction for the SIDAR configuration at 5%, and the integrated γ-ray beam intensity with uncertainties between 4.5% (at 9 and 10 MeV) and 10% (at 4.4 and 4.51 MeV). The cross-section measurements reported in [32] are in disagreement with both earlier data sets [6, 16] if only the reported statistical uncertainties are considered.

The experimental astrophysical S factor for ^{3}H$(\alpha,\gamma)^7$Li$_{g.s.}$ plotted in Fig. 4, calculated from the experimental data using the principle of detailed balance from Eq. 1, was analyzed within the R-matrix formalism with the AZURE2 code [40, 41].

The experimental data in Fig. 4 are fairly well reproduced by the R-matrix result over the entire energy range. The extrapolated astrophysical S factor also agrees well with the lower energy experimental data of Brune *et al.* [37]. This agreement supports the reasonability of the R-matrix extrapolation below the resonant state at $E_x = 4.652$ MeV in ^{7}Li, based on the fitting at the higher energy range. However, the agreement of the present extrapolated result with the data of Brune *et al.* should be treated within the uncertainties of the lowest experimental data points and doesn't solve the disagreement between Brune *et al.* and the theoretical models [35, 36].

Performance of silicon-strip detectors in γ-ray beam was demonstrated in this experiment. The risks from background-induced electron response in silicon-strip detectors is substantial and must be minimized through careful design of the experiment. Available options include the provision for thinner detectors and minimizing the electron-induced background from Compton scattering in materials in and around the chamber as discussed in Section 2.4.

A new measurement of the ^{7}Li$(\gamma,t)^4$He ground-state cross section between $E_\gamma = 3.7$ and 6 MeV was approved by the HIγS Program Advisory Committee and is scheduled to be carried out in Spring 2023.

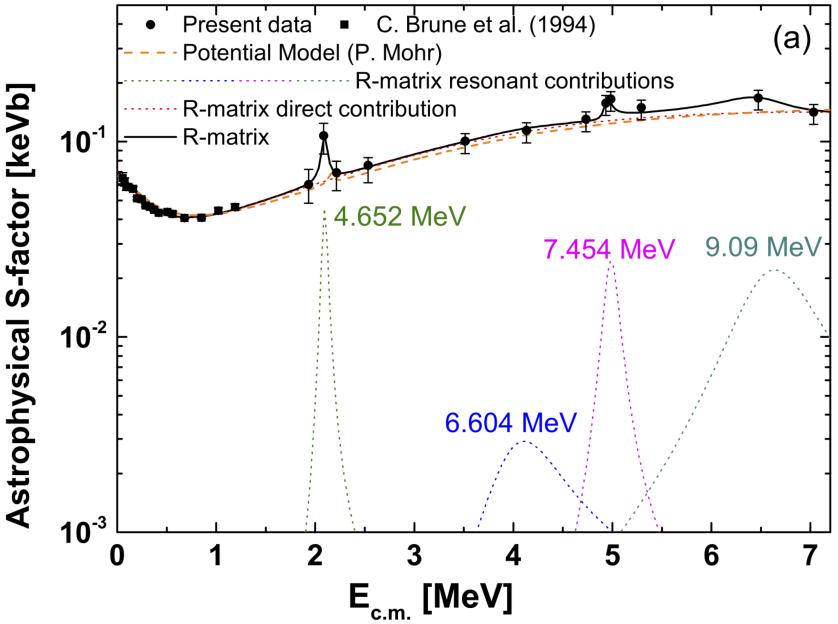

Fig. 4 *R*-matrix fit to the ground state S factor data from experimental data of Munch et al. [32] (Present data). Direct contribution and individual resonance contributions (dotted lines), total contribution (solid line).

2.4 Challenges and future with silicon detector arrays and γ-ray beams

A fundamental limitation of using charged-particle detectors located outside of the target is that the reaction products must be able to get out of the target. Ideally, the energy distribution of these product will form a peak (or peaks) to help kinematically distinguish them from backgrounds (see below). However, due to the electronic energy losses experienced by charged particles traversing the target, these distributions are necessarily spread out due to interactions at different depths in the target. The acceptable energy spread then places a limit on the target thickness [N_t in Eq. (2)]. A further challenge is that the most astrophysically-interesting energies are usually the lowest ones measurable, where the energy losses are the largest.

The potential impact of electron-induced backgrounds in silicon detector arrays operated at γ-ray beam infrastructures can be as high as compromising all data below 1 MeV. As electron signals are proportional to detector thickness, long range energetic electrons will create larger signals in thicker detectors. Therefore, the solution is using detectors as thin as needed to barely

stop the particles of interest for a given experiment. However, most experiments involve the measurement of an excitation function using a range of gamma beam energies, so detector choice is limited by the energies associated with the highest energy point on the excitation function. For experiments on light targets, such as the $^{7}\mathrm{Li}(\gamma, t)^{4}\mathrm{He}$ experiment, both reaction products from photo-disintegration can escape the target and be detected. This can provide substantial (1-2 orders of magnitude) suppression of backgrounds, which are not inherently spatially correlated. However, for most target nuclides, only the ejected light-ions (protons, alphas) can be detected, as the low-energy heavy recoil stops in the target volume. For (γ,p) and (γ,α) reactions at sufficient energies, particle identification using charged particle telescopes can be used to separate protons and alphas from the background electron signals. However, at very low gamma energies, the ejectiles will have insufficient energy to fully penetrate a transmission detector. However, in this limit, a thicker detector can still be employed behind the thinner detector to act as a veto for electrons which pass through both detectors (which includes those from the target, and from scattering on elements close to the beam axis).

Based on the data already obtained at HIγS there is clear need for separation between the light-ions and electrons, in particular in the region of 300 keV to 1 MeV deposited energy. Pulse shape discrimination (PSD) algorithms could extend conventional, previously demonstrated Pulse Shape Analysis for light-ion particle identification [42]. Future PSD developments should improve PSD algorithms for both rise-time and current techniques for electron light-ion discrimination in silicon. It may also be possible to use the time of flight of the charged particles to assist with particle identification and background reduction, depending on the time structure of the photon facility.

A number of other steps can be taken to minimize the electron-induced backgrounds from Compton scattering in detectors and other materials in and around the chamber, including careful design of upstream vacuum flanges and vacuum chamber walls, and the location and material of any entrance windows used for the gamma beam into the vacuum system. This is critical for the detection of the low-energy reaction products observed in the photo-disintegration of ^{7}Li and other photon-induced breakup reactions.

Beyond charged-particle-singles experiments, coupled silicon and germanium arrays could be used for particle-gamma coincidence experiments. There has been substantial recent progress in this field, with the development of TIARA [43], TREX [44] and HI-TREX [45], and SHARC [46] - all arrays utilizing Clover germanium detectors, necessitating relatively compact silicon setups. GODDESS [47] is a coupling of the ORRUBA to the large germanium detector arrays Gammasphere and GRETINA. These arrays have larger internal volumes (around 30-cm spheres), which allow for larger silicon arrays to be implemented inside. Though there is insufficient space to mount and instrument large, very highly segmented detectors such as superORRUBA, there is sufficient room for a large resistive-strip array such as ORRUBA. GODDESS

provides ∼1 degree polar angle resolution from ∼15 to ∼165 degrees, with better than 80% azimuthal efficiency. GODDESS is depicted in Fig. 5 and has been operational with Gammasphere and GRETINA for experiments at ATLAS at Argonne National Laboratory. A particle-gamma setup along these lines could be implemented for gamma-induced measurements. Substantial shielding of the array would be needed to protect from Compton scattering sources.

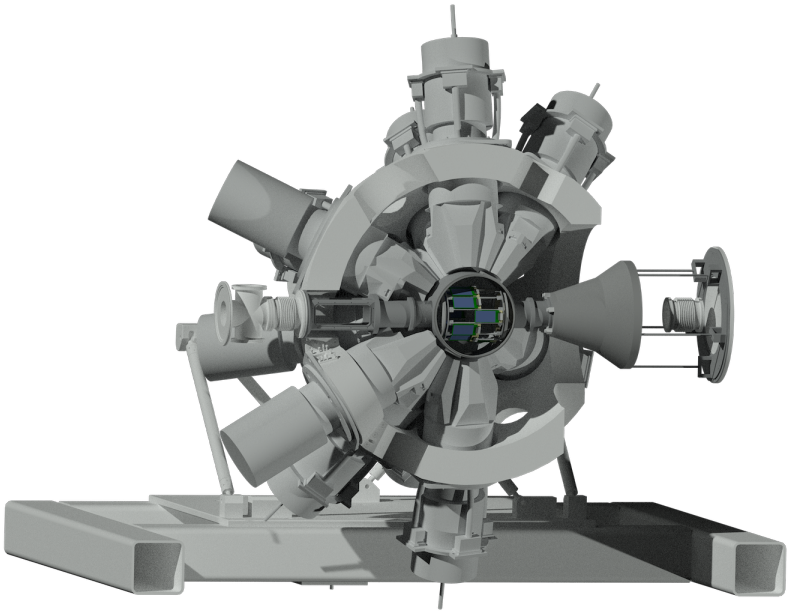

Fig. 5 CAD model of GODDESS implemented with GRETINA.

Potential integration of a compact silicon detector array should be explored with γ-ray and neutron detector arrays currently available at HIγS and with the ELIADE [48] and ELIGANT [49] arrays under development at ELI-NP.

3 Measurements of charged particles from active targets

An overview of photonuclear experiments with detection of charged particles from active-gas targets, specifically using various types of Time Projection Chambers (TPCs), is given is this section.

One of the most promising experimental techniques that can be used with γ-ray beams is to utilize an *active-target* time projection chamber (TPC) detector. The use of TPCs for the measurement of photon-induced reactions is very similar to the use of TPCs for neutron-induced reactions, since the beam

is neutral in both cases. Noteworthy examples TPCs that have been utilized for the measurement of neutron-induced reactions are the Neutron Induced Fission Fragment Tracking Experiment (NIFTE) [50] and the Texas Active Target (TexAT) [51, 52]. These detectors, typically have a solid angle coverage approaching 4π, and permit the use of thick, gaseous targets without worsening the energy resolution. The operation principle is common among these detectors, so a general introduction will be given here, and details of specific detectors will be provided in the following sections where necessary.

Upon a photon-induced interaction inside the gaseous medium, the reaction products propagate through the gas. In doing so, they ionise molecules along their tracks, and lose energy according to their characteristic Bragg curves. The whole gas system is typically kept inside a highly uniform electric field, under the influence of which, the ionisation electrons drift towards an anode plane. This is followed by an electron multiplication stage to produce a measurable signal. The spatial distribution of electrons is measured, along with their times of arrival at the readout plane, and are used to reconstruct the track in three dimensions.

Measurements of the photo-disintegration of ^{3}He and ^{4}He made at the National Institute of Advanced Industrial Science and Technology (AIST) are first discussed in section 3.1. The quest to measure the $^{12}C(\alpha,\gamma)^{16}O$ reaction cross section is briefly reviewed in Section 3.2, followed by a review of a recent experiment to measure the $^{16}O(\gamma,\alpha)^{12}C$ cross section in Section 3.3. Recent instrument developments and prospects for lowering the uncertainty on the $^{12}C(\alpha,\gamma)^{16}O$ reaction cross section are discussed in section 3.4.

3.1 Previous photon-induced measurements with active-gas targets

Photon-induced studies with detection of charged particles from active-gas targets are quite recent, starting only a few years after the beginning of the third millennium. Yet they have proven to be a valuable tool for various studies in nuclear astrophysics.

The Greisen-Zatsepin-Kuz'min (GZK) horizon of helium [53, 54] is a key parameter in determining the contribution of Ultra-High Energy Cosmic Rays (UHECRs) with directions pointing to nearby sources. Analytical and numerical estimates of this parameter, along with Monte Carlo simulations of UHECR propagation are typically based on fits to helium photo-disintegration cross-section measurements and rely on a precise description of the giant dipole resonance (GDR) near threshold.

The first simultaneous measurements of the two-and three-body photo-disintegration cross-sections of ^{4}He in this GDR energy region were performed at the National Institute of Advanced Industrial Science and Technology (AIST) in 2005 using a pulsed-laser Compton backscattering (LCS) photon beam [7]. At AIST, the photon source was developed by using the 800 MeV electron storage ring TERAS and an external Nd:YAG laser in 1985 [55] and covers a 2−40 MeV γ-ray energy range.

The charged fragments from the photo-disintegration of ^{4}He were detected using a Time Projection Chamber(TPC) with a 4π acceptance and 100% efficiency [56] meaning that particle tracks could be observed on an event-by-event basis. The TPC was contained in a vessel of 244 mm inner diameter and 400 mm length and a gas mixture of natural helium (80%) and CH_4 (20%) with a total pressure of 1000 Torr was utilized as the active target. The TPC consisted of a 60×60 mm^2 drift region with a length of 250 mm, and a multiwire proportional counter (MWPC) read-out plane. Electrons resulting from ionisation of the charged particle tracks drift in the uniform electric field towards the read-out plane. The MWPC consisted of one anode plane, sandwiched between two cathode planes. Each plane had 30 wires with a spacing of 2 mm. To obtain two dimensional track information of a charged fragment at the read-out plane, cathode wires in front of and behind the anode plane were aligned in the x and y directions, respectively. The z orientation of a track was determined by measuring the drift time of the ionisation electrons with a time to digital converter.

Using this set-up, data from the three-body ^{4}He(γ, pn) process yielded a cross section of 0.04 ± 0.01 mb at $E_\gamma = 29.8$ MeV, in good agreement with previous experiments. However, the larger ^{4}He(γ, p) and ^{4}He(γ, n) cross sections were found to increase with energy up to 29.8 MeV, giving a GDR shape and position in strong disagreement with numerous previous measurements. The same ^{4}He photo-disintegration cross sections were later measured again in 2010 by the same group at AIST [57], which confirmed their earlier findings.

Using the same TPC, a later measurement in 2006 at AIST explored the cross sections of the ^{3}He(γ, p)d and ^{3}He$(\gamma, pp)n$ reactions [8]. The photo-disintegration cross sections were actually first directly measured in 1965 [58] with a cloud chamber to track the proton and deuteron reaction products. The 2006 measurements were performed using mono-energetic pulsed γ-rays at $E_\gamma = 10.2$ and 16.0 MeV produced by the LCS photon beam at AIST. These high-precision experimental results for photo-disintegration were compared with theoretical predictions for the three-body reaction processes. While at 16.0 MeV the experimental data and theory agree to 12%, a larger discrepancy was observed at 10.2 MeV. The authors point that more high-precision (γ, p) and (γ, pp) cross section data for a larger number of incident photon energies are needed for the comparison with theoretical predications.

3.2 The quest for the ^{12}C$(\alpha, \gamma)^{16}$O cross section

There is no reaction in nuclear astrophysics as important as ^{12}C$(\alpha, \gamma)^{16}$O, for determining the C/O ratio in the Universe and with so much experimental and theoretical work carried out in the last 60 years. Measuring this cross section has presented significant experimental challenges, and have pushed the limits of novel state-of-the-art techniques. Some data sets have been beset with uncharacterized uncertainties, and often results have been conflicting and difficult to reconcile. This issue is highlighted by the apparent disagreement between

some direct measurements of $^{12}C(\alpha,\gamma)^{16}O$, using γ-ray detectors, and a fundamental prediction of quantum mechanics. As we will describe below, precision measurements of charged-particle angular distributions using state-of-the-art TPCs can contribute significantly to our understanding of the $^{12}C(\alpha,\gamma)^{16}O$ cross section at astrophysical energies.

A astrophysical energies, the $^{12}C(\alpha,\gamma)^{16}O$ reaction rate is dominated by the transition to the ground state of ^{16}O, i.e. the $^{12}C(\alpha,\gamma_0)^{16}O$ channel. Differential cross sections for this transition from past experiments [59–66] have been fitted with [59, 67]

$$\frac{d\sigma}{d\Omega} = \frac{1}{4\pi}\Bigg[\sigma_{E1}(1-P_2)+\sigma_{E2}(1+\frac{5}{7}P_2-\frac{12}{7}P_4) + 6\cos(\phi_{12})\sqrt{\frac{\sigma_{E1}\sigma_{E2}}{5}}(P_1-P_3)\Bigg], \tag{3}$$

where σ_{E1} and σ_{E2} are the $E1$ and $E2$ multipole contributions to the ground state cross section, ϕ_{12} is the relative phase between the $E1$ and $E2$ capture amplitudes, and P_ℓ are the Legendre polynomials of order ℓ evaluated at the cosine of the c.m. emission angle of the photon. Values of ϕ_{12} extracted from these measurements of $^{12}C(\alpha,\gamma_0)^{16}O$ should agree with the theoretical prediction [59, 67] of $\phi_{12} = \delta_2 - \delta_1 + \tan^{-1}\eta/2$. Here, δ_1 and δ_2 are $\alpha + {}^{12}C$ elastic scattering phase shifts, and η is the Sommerfeld parameter. This theoretical prediction is known accurately because the elastic scattering phase shifts have been measured to high precision [68]. The theoretical prediction for ϕ_{12} is a consequence of the Watson theorem, which is derived assuming unitarity of the scattering matrix [69–71]. It is valid when the capture cross section is small and is the only open reaction channel.

The consistency of the extracted ϕ_{12} values with the theoretical prediction provides a stringent cross check on the measured differential cross sections. It is also important that various experimental effects, such as the finite geometry of the detection system and c.m. motion, are taken into account [70, 72]. The extracted ϕ_{12} values from previous measurements are shown in Fig. 6. At energies of $E_{cm} < 1.6$ MeV [65, 66], ϕ_{12} was measured to be in agreement with the theoretical prediction [59, 67]. In this energy region, the $E1/E2$ ratio and ϕ_{12} are almost constant, but the uncertainties in ϕ_{12} are relatively large due to the extreme difficulty of the measurements.

In contrast, in the energy region of $1.8 < E_{cm} < 2.8$ MeV, both the $E1/E2$ ratio and ϕ_{12} vary rapidly due to the broad 9.58 MeV 1^- resonance in ^{16}O. This resonance enables the measurements in this region to have much smaller uncertainties but, as one can see from Eq. (3), the dominance of the $E1$ component also reduces the sensitivity to ϕ_{12}. As shown in Ref. [72], the variation of ϕ_{12} leads to subtle changes in the measured angular distributions. Here, Assunção et al. [63] observed substantial disagreement with the theoretical prediction of ϕ_{12}. Ouellet et al. [61] noted that they were unable to extract ϕ_{12} from their angular distributions measured between 1.9−2.4 MeV. The data of Dyer and

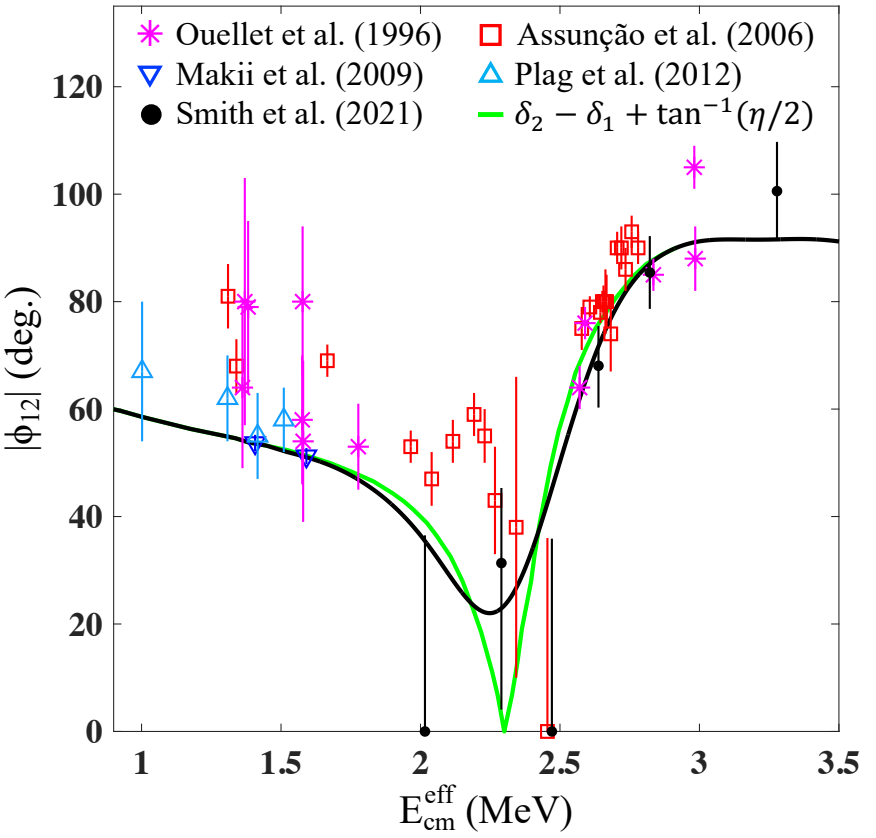

Fig. 6 Plot of ϕ_{12} values extracted for the $^{12}C(\alpha,\gamma_0)^{16}O$ reaction. Data from Refs. [59] and [60] are excluded due to 100% error bars. The solid green curve is the theoretical prediction of Eq. (3) based on the phase shifts from Refs. [68, 73, 74], and the solid black curve is the theoretical prediction convolved with the 300-keV energy resolution of the experiment of Smith et al. [75].

Barnes [59] are measured mostly with 100% error bars in this region, as are the data of Redder et al. [60]. Thus, so far, no measurements of $^{12}C(\alpha,\gamma_0)$ exhibit the predicted strong variation of ϕ_{12} over the 1^- resonance region. The observed discrepancy between some previous data and theory across the 1^- resonance, is a disagreement with a fundamental prediction of quantum theory. It should not be overlooked, and clearly points to underestimated or unaccounted systemic uncertainties in some previous experiments.

Furthermore, the direct measurements of the $^{12}C(\alpha,\gamma_0)$ reaction using gamma detectors [63] were retrospectively re-analyzed [71, 72], and significant uncertainties were noted. Large backgrounds in the measured γ-ray spectra lead to uncertainties in the measured angular distributions, and the extracted cross sections [71]. The large uncertainties deduced for Ref. [63], (induced, for example, by in-beam neutrons), and similar data [76], lead to uncertainties in

the R-Matrix extrapolation to astrophysical energies [77]. For reliable calculations of reaction rates at stellar conditions, new measurements with lower backgrounds are required. In the latest extrapolation to astrophysical energies, deBoer et al. [77] analyzed the global data − not just direct measurements of $^{12}C(\alpha,\gamma)$ − and concluded that at the Gamow window, a "level of uncertainty ∼10% may be in sight". The review of deBoer et al. has also clearly made the case that improved experimental data are needed.

3.3 Recent $^{16}O(\gamma,\alpha)^{12}C$ measurement with OTPC at HIγS

Recently, the $^{12}C(\alpha,\gamma_0)^{16}O$ cross section was inferred using an entirely new method, where the inverse $^{16}O(\gamma,\alpha)^{12}C$ photo-disintegration reaction was measured using γ-ray beams and an Optical Time Projection Chamber (OTPC) [75]. Measurements were focused on $E_{cm} = 2.0-2.6$ MeV, because, as previously noted, a broad 1^- resonance (corresponding to the 9.59-MeV state in ^{16}O) enhances the cross section in this region, making higher statistics measurements more viable. Secondly, because the shape of the angular distributions in this region are less sensitive to the value of ϕ_{12}, it is an ideal testing ground for determining the accuracy of measured angular distributions. These successful proof-of-principle measurements have provided motivation for extending similar measurements down toward lower energies and with a newer detector.

Quasi mono-energetic γ-ray beams of circular polarization were produced at HIγS. The γ-ray beam energy is controlled by varying the wavelength of the free-electron-laser (FEL) and the electron energy [4]. A circularly polarized beam was chosen in order to limit the wear of optical components, given the length of the experiment and high beam intensity of $\sim 10^8\gamma$/s. The beam was varied from $E_\gamma = 9.01 - 10.43$ MeV and had a spread of ∼3% at FWHM.

In this experiment, instead of measuring the fusion of α and ^{12}C to form ^{16}O, γ-ray beams were used to measure the time reversed process of $^{16}O(\gamma,\alpha)^{12}C$ photo-disintegration. As noted in section 1, the photo-disintegration cross section is directly related to the capture cross section via the principle of detailed balance and is larger by a factor of ∼50 in this energy region. The tracks of the α and ^{12}C reaction products were measured inside in the Time Projection Chamber detector operating with a mixture of CO_2 (80%) and N_2 (20%) gas at 100 Torr pressure. The details of the detector operation are discussed in Ref. [78]. The OTPC permitted the ^{16}O photo-disintegration events to be unambiguously identified with very low background and measured with high efficiency, over a range of polar angles.

As the reaction products propagate through the gas mixture, they ionize atoms along their tracks, losing energy according to their characteristic Bragg curves. The ionization electrons drift in the OTPC under the influence of a uniform electric field. The drift electrons are then multiplied by a stronger electric field (∼10× larger than the drift field), giving rise to an avalanche and producing scintillation light. The light was detected by four photomultiplier

tubes (PMTs) that surrounded the top of the TPC, and the signal was digitized using a 100 MHz ADC. This constitutes the vertical *time projection* of the track. At the same time, optical photons propagate through the opto-electronic chain and are focussed onto a CCD camera, which photographs the track *in plane*.

The combination of the time projection and CCD image allowed detailed angular distributions for the $^{16}O(\gamma,\alpha)^{12}C$ reaction to be measured with an unprecedented θ angular resolution of $\sim 2^\circ$, and over a large range of polar angles. Background events recorded by the OTPC include cosmic rays, Compton electrons, $^{14}N(\gamma,p)$, $^{17,18}O(\gamma,\alpha)$, and $^{12}C(\gamma,\alpha)^{8}Be$ reactions. The majority of background events could be removed by examination of the energy deposited, the position of the tracks within the detector, and by measuring the stopping power of the ionizing particles.

The $^{12}C(\alpha,\gamma_0)^{16}O$ cross sections measured using the OTPC, along with the global data set of previous direct measurements, are shown in Fig. 7. Broad agreement with the global data set, comprising of data gathered from direct $^{12}C(\alpha,\gamma_0)$ measurements, is seen across the whole energy range.

Note that the measurements of Ref. [75] are labelled at "effective" centre-of-mass energies. Since the γ-ray beam is broad in energy (approximately 300 keV FWHM in this case), the rapidly-varying cross section can change significantly across the width of the beam. Therefore, the "effective energies" of these measurements are defined as the beam energy averaged over the width of the broad γ-ray beam, weighted by the global cross section data [72]. Similarly, the cross sections themselves are "effective cross sections" for this same reason. Cross sections were corrected by a factor based on the gamma beam width and global cross section data, using the method described in Ref. [72].

An example angular distribution obtained during this experiment is shown in Fig. 8. Due to the impressive 2° angular resolution, an unbinned maximum log-likelihood fit to the data was performed in order to extract σ_{E1}, σ_{E2}, and ϕ_{12}. Data are binned in Fig. 8 for visualization purposes only. The extracted ϕ_{12} values are shown in Fig. 6 and follow the expected trend within the (sometimes large) statistical uncertainties.

3.4 Challenges and future with active-gas targets and γ-ray beams

One limitation of γ-ray beam experiments for nuclear astrophysics using current facilities such as HIγS, arises from the spread in the incident photon beam energies. The extraction of the cross section thus requires that the energy distribution of the photon beam be well characterized and that the energy dependence of the cross section is known. As noted in section 3.3, the cross sections of [75] required significant correction due to the beam energy spread (3% at FWHM).

However, this issue is not unique to γ-ray beam experiments. In charged particle experiments, particularly at low energies where cross sections are smaller, relatively thick targets are required and the energy loss in the target

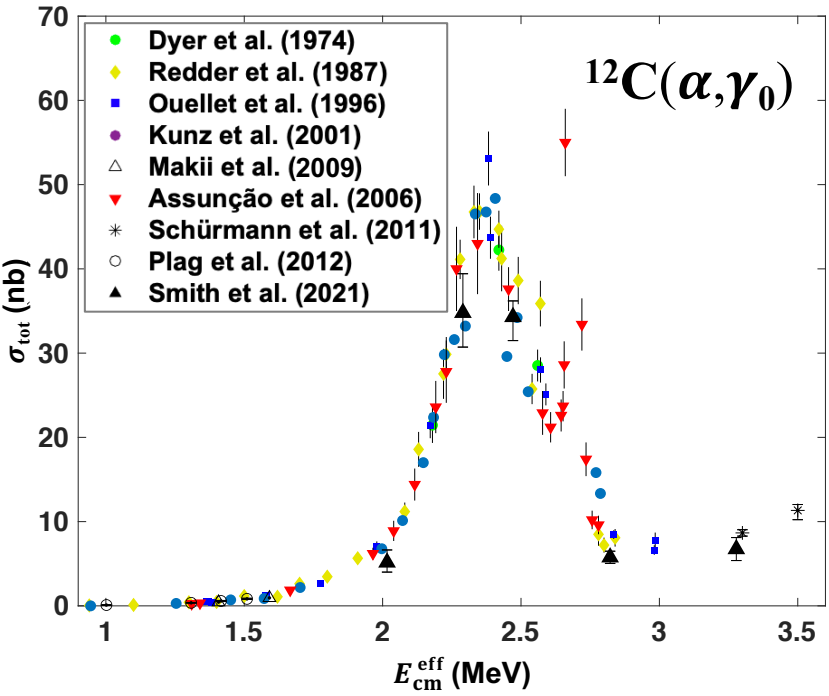

Fig. 7 The cross section for the $^{12}C(\alpha,\gamma_0)^{16}O$ reaction showing data from Refs. [59–66, 75]. A linear scale for the cross section is used here to optimize the comparison of the recent Smith et al. (2021) [75] data to other experiments.

material is significant. For example, the lowest-energy measurement of Ref. [63] was performed with an incident beam energy of $E_\alpha = 1.85$ MeV, where the energy loss in their implanted carbon targets was about 180 keV in the c.m. system. Note also that the $^{12}C(\alpha,\gamma_0)^{16}O$ cross section varies by about factor of 2.5 over this energy spread. Such variations require corrections to the extracted cross sections and careful evaluation of the effective centre-of-mass energies [72]. As we look towards new facilities, such as ELI-NP, which should offer a 0.5% beam energy resolution, higher precision measurements over narrower energy ranges will be possible.

There are other approaches to dealing with the γ-ray beam energy spread in that may be useful in the future. One idea is to utilize the fact that the beam energy spread at Compton backscattering facilities primarily arises from the angle-dependence of the Compton scattering kinematics. One can thus use the location of the vertex of the events in the TPC to infer what the photon energy was on an event-by-event basis. This method would also allow more open collimation on the gamma beam to used, which increases the photon flux. Another approach is to use the energy detected in the TPC to infer the photon energy, again on an event-by-event basis. Both of these methods are contingent upon the availability of a high-performance TPC that can measure

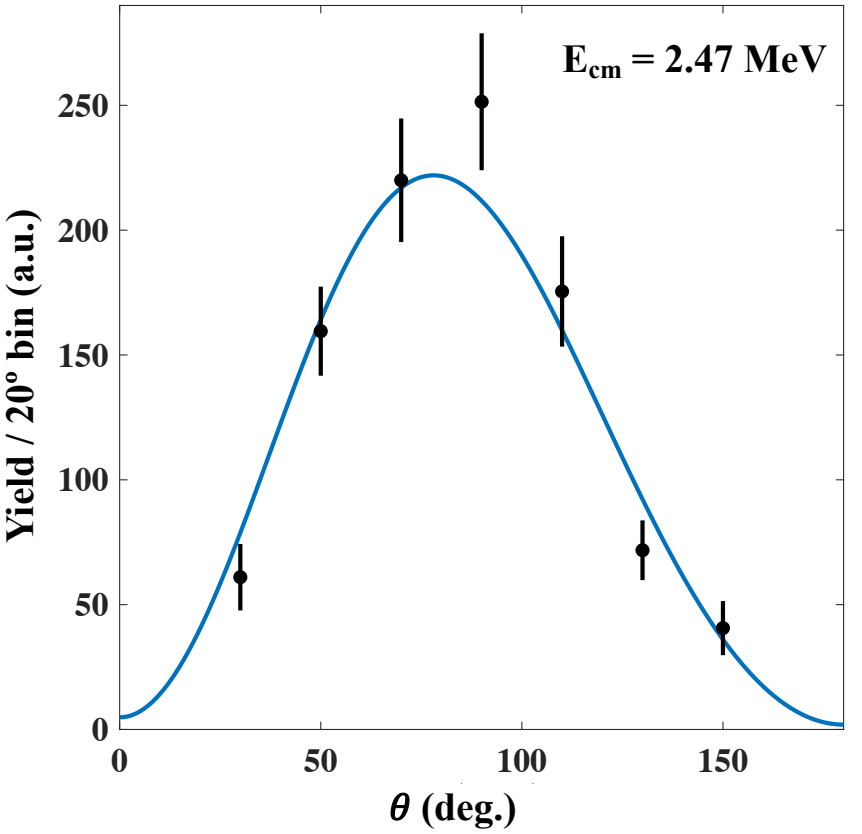

Fig. 8 A measured angular distribution using the OTPC at an effective centre-of-mass energy of 2.47 MeV [75].

particle tracks and energies with resolutions on the order of 1 mm and 0.5%, respectively.

In terms of $^{12}C(\alpha,\gamma)$, further improvements are underway. The work of Ref. [75] utilized a CO_2 + N_2 gas target. The Q-values for the $^{12}C(\gamma,\alpha)2\alpha$ and $^{16}O(\gamma,\alpha)^{12}C$ reactions are separated by just 114 keV, which means that the two reactions were indistinguishable based on the energies they deposited in the TPC (due to the $\sim$ 300 keV beam width and the $\sim$ 100 keV TPC energy resolution [78]). Instead, the two event types were separated using a complicated lineshape analysis of the measured time projections – see the methods section of Ref. [75]. For each event, the theoretical lineshapes for energy losses of ^{12}C + α and also three alpha particles, corresponding to ^{16}O and ^{12}C photo-disintegration events, were fitted to the time projection. Comparison of the χ^2 of each fit was used to classify each event.

However, events with small out-of-plane angles were indistinguishable using this method, due to the time projection being too short. This meant that fiducial volume cuts were employed, which had to be corrected for when evaluating total cross sections. This lowered the efficiency of the set-up, reducing the total number of counts in each angular distribution, and increasing the statistical uncertainties on the important extracted parameters.

More recently, the experiment was repeated with γ-beam energies from 9.38 to 9.8 MeV using an alternative $N_2O + N_2$ gas target in the optical TPC. Removal of the carbon from the target theoretically improves this experiment; fiducial volume cuts are not required and higher statistics may be obtained. However, this new approach is not without its challenges. The characteristics of the TPC while operating with a nitrous oxide gas are highly sensitive to the drift voltage-pressure ratio. Furthermore, nitrous oxide is an attaching gas, where electrons in the TPC are captured, producing negative ions during their drift. These ions may then later decay, releasing the electrons. As such, distortions in the time projections are obtained and careful modelling of the electron-N_2O interactions are required in order to accurately extract polar angles. Analysis is underway and a publication is expected in 2023.

In a further advance forward for measuring the $^{12}C(\alpha,\gamma)$ cross section, recent measurements were made at the HIγS facility in 2022 using a new electronic Time Projection Chamber, built by the University of Warsaw [79–81]. The new measurements were conducted with γ-beams with energies from 8.51−13.9 MeV. The active target consisted of a pure CO_2 gas contained inside the TPC.

The Warsaw TPC has active dimensions of 33 × 20 cm^2 (readout plane) × 20cm (drift) and is contained inside a vacuum vessel. The amplification structure consists of three 50 µm-thick Gas Electron Multiplier (GEM) foils, which sit above a planar anode, segmented into 1.5-mm-thick strips along 3 axes (U, V, W), each oriented 60° with respect to each other. These three independent linear sets of strips allow for redundant readout and requires around 1000 electronics channels. These are read by General Electronics for TPCs (GET) technology front-end cards [82] with custom FPGA readout developed at the University of Warsaw. The arrays of strips enable the electron hit positions in two dimensions to be found by generating virtual pixels. The time distribution of the charge collected at the anode, combined with the drift velocity of the electrons in the CO_2, allows the determination of the vertical coordinate. An example oxygen-16 photo-disintegration event as measured in the Warsaw TPC may be seen in Fig. 9.

Importantly, the electronic TPC permitted an event readout of up to 80 Hz without zero suppression; almost two orders of magnitude higher than the Optical TPC discussed in Section 3.3. Therefore, higher statistics were measured, which will, in principle, reduce statistical uncertainties on important parameters extracted from fits to angular distributions. Furthermore, due to the UVW readout, and improved spatial resolution, events can be recorded in 4π efficiency, without the need for fiducial volume cuts.

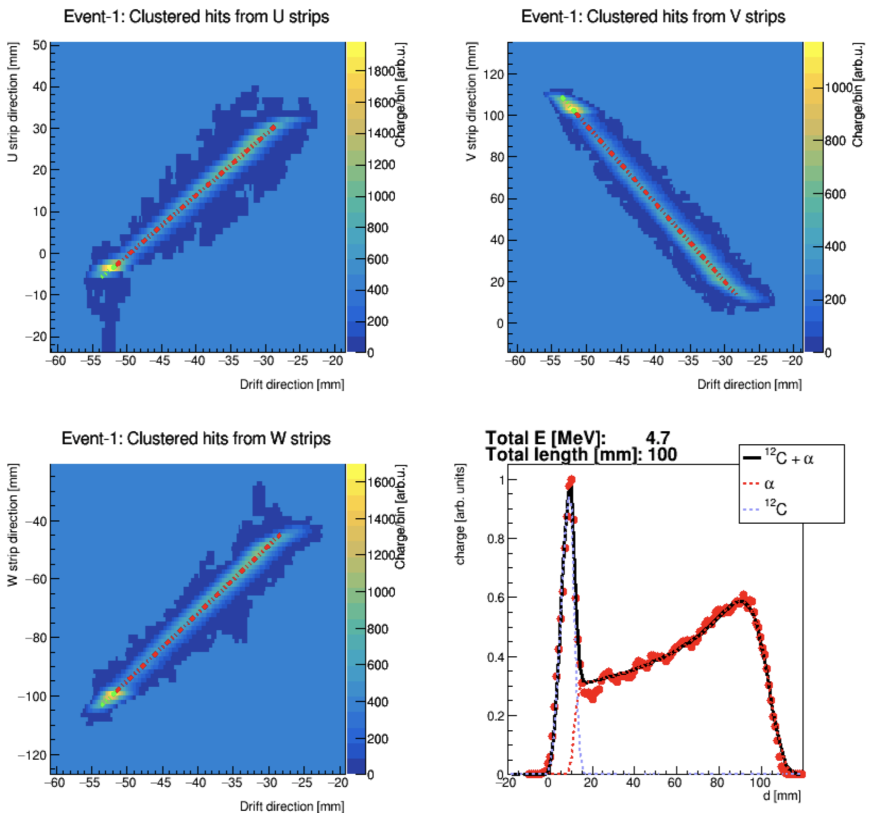

Fig. 9 A typical event identified as oxygen-16 photo-disintegration, shown in UVW space, measured at Eγ = 12.3 MeV [83]. The lower right panel shows the charge deposited by the particles along the track, and a fit by the theoretical dE/dx curve. The offset in the horizontal scale is arbitrary.

4 Conclusions and Outlook

Studies of photonuclear reaction cross sections became part of the mainstream experimental nuclear physics in the last 20 years with the help of mono-energetic γ-ray beam facilities and improved detection methods. However, charged-particle detection from photon-induced reactions had a slow evolution and the field is only now emerging on the experimental stage. Measurements of (γ, p) and (γ, α) photonuclear reaction cross sections have the potential to offer the solution to several key reactions in nuclear astrophysics. The paper highlights the recent ^{7}Li$(\gamma, t)^{4}$He measurement at HIγS with implications in Big Bang nucleosynthesis and for paving the way to solve in the near future the disagreement between the experimental and theoretical capture cross section in the mirror α-capture reactions ^{3}H$(\alpha, \gamma)^{7}$Li and ^{3}He$(\alpha, \gamma)^{7}$Be. Another highlight is the recent result from a measurement of the ^{16}O$(\gamma, \alpha)^{12}$C cross section

using an optical time projection chamber at HIγS, part of the quest to measure the very important $^{12}C(\alpha,\gamma)^{16}O$ reaction cross section.

Two main experimental directions were identified for detecting charged particles from photon-induced reactions: measurements from solid targets using silicon-strip detectors, and measurements with active gas targets within time projection chambers. The evolution of silicon-strip detector arrays over the last 20 years allowed the implementation of a large area silicon-detector array at HIγS for the recent $^{7}Li(\gamma,t)^{4}He$ measurement and the development of the ELISSA setup at ELI-NP. Future developments will integrate a compact silicon detector array with γ-ray and neutron detector arrays currently available at HIγS and ELI-NP. The use of an optical time projection chamber with a mixture of CO_2 (80%) and N_2 (20%) gas permitted the ^{16}O photo-disintegration events to be unambiguously identified with very low background and measured with high efficiency. Recent operation of the Warsaw active-target electronic TPC at HIγS sets the stage for future studies of the $^{16}O(\gamma,\alpha)^{12}C$ reaction cross section and other reactions of interest for nuclear astrophysics.

HIγS continues to be the main facility for performing experiments while VEGA at ELI-NP is still in implementation phase. There are several experiments measuring charged particles approved to run at HIγS in the next years, pushing the limits on photo-disintegration cross sections for light nuclei (^{7}Li), p-process reactions (^{102}Pd and ^{112}Sn), and the $^{16}O(\gamma,\alpha)^{12}C$ cross section.

Acknowledgments. This work is supported by the Romanian Ministry of Research, Innovation and Digitalization, project no. PN-III-P4-PCE-2021-1024 and PN 23 21 01 06; the U.S. Department of Energy, Office of Science, Nuclear Physics program, grants no. DE-FG02-94ER40870, DE-FG02-88ER40387, and DE-AC05-00OR22725; the U.S. Department of Energy, National Nuclear Security Agency, grant no. DE-NA0004065; and the UK STFC, grant no. ST/V001086/1.

References

[1] Strauch, K.: Recent studies of photonuclear reactions. Annual Review of Nuclear Science **2**(1), 105–128 (1953). https://doi.org/10.1146/annurev.ns.02.120153.000541

[2] Zilges, A., Balabanski, D.L., Isaak, J., Pietralla, N.: Photonuclear reactions — From basic research to applications. Progress in Particle and Nuclear Physics **122**, 103903 (2022). https://doi.org/10.1016/j.ppnp.2021.103903

[3] Howell, C.R., Ahmed, M.W., Afanasev, A., Alesini, D., Annand, J.R.M., Aprahamian, A., Balabanski, D.L., Benson, S.V., Bernstein, A., Brune, C.R., Byrd, J., Carlsten, B.E., Champagne, A.E., Chattopadhyay, S., Davis, D., Downie, E.J., Durham, J.M., Feldman, G., Gao, H., Geddes, C.G.R., Grießhammer, H.W., Hajima, R., Hao, H., Hornidge, D., Isaak, J.,

Janssens, R.V.F., Kendellen, D.P., Kovash, M.A., Martel, P.P., Meißner, U.-G., Miskimen, R., Pasquini, B., Phillips, D.R., Pietralla, N., Savran, D., Schindler, M.R., Sikora, M.H., Snow, W.M., Springer, R.P., Sun, C., Tang, C., Tiburzi, B., Tonchev, A.P., Tornow, W., Ur, C.A., Wang, D., Weller, H.R., Werner, V., Wu, Y.K., Yan, J., Zhao, Z., Zilges, A., Zomer, F.: International workshop on next generation gamma-ray source. Journal of Physics G: Nuclear and Particle Physics **49**(1), 010502 (2021). https://doi.org/10.1088/1361-6471/ac2827

[4] Weller, H.R., Ahmed, M.W., Gao, H., Tornow, W., Wu, Y.K., Gai, M., Miskimen, R.: Research opportunities at the upgraded HIγS facility. Prog. Part. Nucl. Phys. **62**, 257–303 (2009). https://doi.org/10.1016/j.ppnp.2008.07.001

[5] Baur, G., Bertulani, C.A., Rebel, H.: Coulomb dissociation as a source of information on radiative capture processes of astrophysical interest. Nuclear Physics A **458**(1), 188–204 (1986). https://doi.org/10.1016/0375-9474(86)90290-3

[6] Junghans, G., Bangert, K., Berg, U.E.P., Stock, R., Wienhard, K.: The photodisintegration of ^{6}Li and ^{7}Li. Z. Physik A **291**(4), 353–365 (1979). https://doi.org/10.1007/BF01408386

[7] Shima, T., Naito, S., Nagai, Y., Baba, T., Tamura, K., Takahashi, T., Kii, T., Ohgaki, H., Toyokawa, H.: Simultaneous measurement of the photodisintegration of ^{4}He in the giant dipole resonance region. Phys. Rev. C **72**, 044004 (2005). https://doi.org/10.1103/PhysRevC.72.044004

[8] Naito, S., Nagai, Y., Shima, T., Makii, H., Mishima, K., Tamura, K., Toyokawa, H., Ohgaki, H., Golak, J., Skibi ński, R., Witała, H., Glöckle, W., Nogga, A., Kamada, H.: New data for total ^{3}He(γ, p)d and ^{3}He(γ, pp)n cross sections compared to current theory. Phys. Rev. C **73**, 034003 (2006). https://doi.org/10.1103/PhysRevC.73.034003

[9] Ugalde, C., DiGiovine, B., Henderson, D., Holt, R.J., Rehm, K.E., Sonnenschein, A., Robinson, A., Raut, R., Rusev, G., Tonchev, A.P.: First determination of an astrophysical cross section with a bubble chamber: The ^{15}N$(\alpha,\gamma)^{19}$F reaction. Physics Letters B **719**(1), 74–77 (2013). https://doi.org/10.1016/j.physletb.2012.12.068

[10] Taleyarkhan, R.P., Archambault, B., Sansone, A., Grimes, T.F., Hagen, A.: Neutron spectroscopy & H*10 dosimetry with tensioned metastable fluid detectors. Nuclear Instruments and Methods in Physics Research Section A: Accelerators, Spectrometers, Detectors and Associated Equipment **959**, 163278 (2020). https://doi.org/10.1016/j.nima.2019.163278

[11] https://www.eli-np.ro/rd2_second.php

[12] Tesileanu, O., Gai, M., Anzalone, A., Balan, C., Bihalowicz, J.S., Cwiok, M., Dominik, W., Gales, S., Ghita, D.G., Janas, Z., Kendellen, D.P., Cognata, M.L., Matei, C., Mikszuta, K., Petcu, C., Pfutzner, M., Matulewicz, T., Mazzocchi, C., Spitaleri, C.: Charged particle detection at ELI-NP. Rom. Rep. in Phys. **68**, 699 (2016)

[13] Lan, H.Y., Xu, Y., Luo, W., Balabanski, D.L., Goriely, S., La Cognata, M., Matei, C., Anzalone, A., Chesnevskaya, S., Guardo, G.L., *et al.*: Determination of the photodisintegration reaction rates involving charged particles: Systematic calculations and proposed measurements based on the facility for Extreme Light Infrastructure-Nuclear Physics. Phys. Rev. C **98**(5), 054601 (2018). https://doi.org/10.1103/PhysRevC.98.054601

[14] Lan, H.Y., Luo, W., Xu, Y., Balabanski, D.L., Guardo, G.L., La Cognata, M., Lattuada, D., Matei, C., Pizzone, R.G., Rauscher, T., Zhou, J.L.: Feasibility of studying astrophysically important charged-particle emission with the variable energy γ-ray system at the Extreme Light Infrastructure–Nuclear Physics facility. Phys. Rev. C **105**, 044618 (2022). https://doi.org/10.1103/PhysRevC.105.044618

[15] Weller, H.R., Ahmed, M.W., Gao, H., Tornow, W., Wu, Y.K., Gai, M., Miskimen, R.: Forward photodisintegration of the deuteron at 10.74 MeV photon energy. Few-Body Systems **1**, 135–141 (1986). https://doi.org/10.1007/BF01077004

[16] Likhachev, V.P., Martins, M.N., da Cruz, M.T.F., Arruda-Neto, J.D.T., Geraldo, L.P., Semmler, R., Dias, J.F.: Triton angular distributions from the $^{7}\mathrm{Li}(\gamma,t)\alpha$ reaction near threshold. Phys. Rev. C **59**, 525–527 (1999). https://doi.org/10.1103/PhysRevC.59.525

[17] Kemmer, J.: Fabrication of low noise silicon radiation detectors by the planar process. Nuclear Instruments and Methods **169**(3), 499–502 (1980). https://doi.org/10.1016/0029-554X(80)90948-9

[18] Davinson, T., Bradfield-Smith, W., Cherubini, S., DiPietro, A., Galster, W., Laird, A.M., Leleux, P., Ninane, A., Ostrowski, A.N., Shotter, A.C., Vervier, J., Woods, P.J.: Louvain–Edinburgh Detector Array (LEDA): a silicon detector array for use with radioactive nuclear beams. Nuclear Instruments and Methods in Physics Research Section A: Accelerators, Spectrometers, Detectors and Associated Equipment **454**(2), 350–358 (2000). https://doi.org/10.1016/S0168-9002(00)00479-4

[19] Bardayan, D.W., Blackmon, J.C., Brune, C.R., Champagne, A.E., Chen, A.A., Cox, J.M., Davinson, T., Hansper, V.Y., Hofstee, M.A., Johnson, B.A., Kozub, R.L., Ma, Z., Parker, P.D., Pierce, D.E., Rabban, M.T., Shotter, A.C., Smith, M.S., Swartz, K.B., Visser, D.W., Woods, P.J.: The astrophysically important 3^{+} state in $^{18}\mathrm{Ne}$ and the $^{17}\mathrm{F}(p,\gamma)^{18}\mathrm{Ne}$

stellar rate. Phys. Rev. C **62**, 055804 (2000). https://doi.org/10.1103/PhysRevC.62.055804

[20] Visser, D.W., Caggiano, J.A., Lewis, R., Handler, W.B., Parikh, A., Parker, P.D.: Particle decay branching ratios for states of astrophysical importance in ^{19}Ne. Phys. Rev. C **69**, 048801 (2004). https://doi.org/10.1103/PhysRevC.69.048801

[21] Murphy, A.S.J., Aliotta, M., Davinson, T., Ruiz, C., Woods, P.J., D'Auria, J.M., Buchmann, L., Chen, A.A., Laird, A.M., Sarazin, F., Walden, P., Fulton, B.R., Pearson, J.E., Brown, B.A.: Level structure of ^{21}Mg: Nuclear and astrophysical implications. Phys. Rev. C **73**, 034320 (2006). https://doi.org/10.1103/PhysRevC.73.034320

[22] Roeder, B.T., McCleskey, M., Trache, L., Alharbi, A.A., Banu, A., Cherubini, S., Davinson, T., Goldberg, V.Z., Gulino, M., Pizzone, R.G., Simmons, E., Spartà, R., Spiridon, A., Spitaleri, C., Wallace, J.P., Tribble, R.E., Woods, P.J.: The Texas–Edinburgh–Catania Silicon Array (TECSA): A detector for nuclear astrophysics and nuclear structure studies with rare isotope beams. Nuclear Instruments and Methods in Physics Research Section A: Accelerators, Spectrometers, Detectors and Associated Equipment **634**(1), 71–76 (2011). https://doi.org/10.1016/j.nima.2011.01.035

[23] Adsley, P., Neveling, R., Papka, P., Dyers, Z., Brümmer, J.W., Diget, C.A., Hubbard, N.J., Li, K.C.W., Long, A., Marin-Lambarri, D.J., Pellegri, L., Pesudo, V., Pool, L.C., Smit, F.D., Triambak, S.: CAKE: the coincidence array for K600 experiments. Journal of Instrumentation **12**(02), 02004 (2017). https://doi.org/10.1088/1748-0221/12/02/T02004

[24] Good, E.C., Sudarsan, B., Macon, K.T., Deibel, C.M., Baby, L.T., Blackmon, J.C., Benetti, C., Esparza, J.C., Gerken, N., Hanselman, K., McCann, G.W., Morelock, A.B., Perello, J.F., Pham, K.H., Rubino, E., Temanson, E., Wiedenhöver, I.: SABRE: The Silicon Array for Branching Ratio Experiments. Nuclear Instruments and Methods in Physics Research Section A: Accelerators, Spectrometers, Detectors and Associated Equipment **1003**, 165299 (2021). https://doi.org/10.1016/j.nima.2021.165299

[25] Pain, S.D., Cizewski, J.A., Hatarik, R., Jones, K.L., Thomas, J.S., Bardayan, D.W., Blackmon, J.C., Nesaraja, C.D., Smith, M.S., Kozub, R.L., Johnson, M.S.: Development of a high solid-angle silicon detector array for measurement of transfer reactions in inverse kinematics. Nuclear Instruments and Methods in Physics Research Section B: Beam Interactions with Materials and Atoms **261**(1), 1122–1125 (2007). https://doi.org/10.1016/j.nimb.2007.04.289. The Application of Accelerators in Research and

Industry

[26] Chesnevskaya, S., Balabanski, D.L., Choudhury, D., Constantin, P., Filipescu, D.M., Ghita, D.G., Guardo, G.L., Lattuada, D., Matei, C., Rotaru, A., State, A.: Performance studies of X3 silicon detectors for the future ELISSA array at ELI-NP. J. Inst. **13**(5), 05006 (2018). https://doi.org/10.1088/1748-0221/13/05/T05006

[27] Engel, G.L., Sadasivam, M., Nethi, M., Elson, J.M., Sobotka, L.G., Charity, R.J.: A multi-channel integrated circuit for use in low- and intermediate-energy nuclear physics—HINP16C. Nuclear Instruments and Methods in Physics Research Section A: Accelerators, Spectrometers, Detectors and Associated Equipment **573**(3), 418–426 (2007). https://doi.org/10.1016/j.nima.2006.12.052

[28] Wallace, M.S., Famiano, M.A., van Goethem, M.-J., Rogers, A.M., Lynch, W.G., Clifford, J., Delaunay, F., Lee, J., Labostov, S., Mocko, M., Morris, L., Moroni, A., Nett, B.E., Oostdyk, D.J., Krishnasamy, R., Tsang, M.B., de Souza, R.T., Hudan, S., Sobotka, L.G., Charity, R.J., Elson, J., Engel, G.L.: The high resolution array (HiRA) for rare isotope beam experiments. Nuclear Instruments and Methods in Physics Research Section A: Accelerators, Spectrometers, Detectors and Associated Equipment **583**(2), 302–312 (2007). https://doi.org/10.1016/j.nima.2007.08.248

[29] Bardayan, D.W., Ahn, S., Blackmon, J.C., Burkhart, A.J., Chae, K.Y., Cizewski, J.A., Elson, J., Hardy, S., Kozub, R.L., Linhardt, L., Manning, B., Matoš, M., Pain, S.D., Sobotka, L.G., Smith, M.S.: Construction and commissioning of the SuperORRUBA detector. Nuclear Instruments and Methods in Physics Research Section A: Accelerators, Spectrometers, Detectors and Associated Equipment **711**, 160–165 (2013). https://doi.org/10.1016/j.nima.2013.01.035

[30] Chipps, K.A., Greife, U., Bardayan, D.W., Blackmon, J.C., Kontos, A., Linhardt, L.E., Matos, M., Pain, S.D., Pittman, S.T., Sachs, A., Schatz, H., Schmitt, K.T., Smith, M.S., Thompson, P.: The Jet Experiments in Nuclear Structure and Astrophysics (JENSA) gas jet target. Nuclear Instruments and Methods in Physics Research Section A: Accelerators, Spectrometers, Detectors and Associated Equipment **763**, 553–564 (2014). https://doi.org/10.1016/j.nima.2014.06.042

[31] Schmidt, K., Chipps, K.A., Ahn, S., Bardayan, D.W., Browne, J., Greife, U., Meisel, Z., Montes, F., O'Malley, P.D., Ong, W.-J., Pain, S.D., Schatz, H., Smith, K., Smith, M.S., Thompson, P.J.: Status of the JENSA gas-jet target for experiments with rare isotope beams. Nuclear Instruments and Methods in Physics Research Section A: Accelerators, Spectrometers, Detectors and Associated Equipment **911**, 1–9 (2018). https://doi.org/

10.1016/j.nima.2018.09.052

[32] Munch, M., Matei, C., Pain, S.D., Febbraro, M.T., Chipps, K.A., Karwowski, H.J., Diget, C.A., Pappalardo, A., Chesnevskaya, S., Guardo, G.L., Walter, D., Balabanski, D.L., Becchetti, F.D., Brune, C.R., Chae, K.Y., Frost-Schenk, J., Kim, M.J., Kwag, M.S., La Cognata, M., Lattuada, D., Pizzone, R.G., Rapisarda, G.G., Turturica, G.V., Ur, C.A., Xu, Y.: Measurement of the ^{7}Li$(\gamma, t)^{4}$He ground-state cross section between $E_\gamma = 4.4$ and 10 MeV. Phys. Rev. C **101**, 055801 (2020). https://doi.org/10.1103/PhysRevC.101.055801

[33] Bemmerer, D., Confortola, F., Costantini, H., Formicola, A., Gyürky, G., Bonetti, R., Broggini, C., Corvisiero, P., Elekes, Z., Fülöp, Z., Gervino, G., Guglielmetti, A., Gustavino, C., Imbriani, G., Junker, M., Laubenstein, M., Lemut, A., Limata, B., Lozza, V., Marta, M., Menegazzo, R., Prati, P., Roca, V., Rolfs, C., Alvarez, C.R., Somorjai, E., Straniero, O., Strieder, F., Terrasi, F., Trautvetter, H.P.: Activation measurement of the ^{3}He$(\alpha, \gamma)^{7}$Be cross section at low energy. Phys. Rev. Lett. **97**, 122502 (2006). https://doi.org/10.1103/PhysRevLett.97.122502

[34] Di Leva, A., Gialanella, L., Kunz, R., Rogalla, D., Schürmann, D., Strieder, F., De Cesare, M., De Cesare, N., D'Onofrio, A., Fülöp, Z., Gyürky, G., Imbriani, G., Mangano, G., Ordine, A., Roca, V., Rolfs, C., Romano, M., Somorjai, E., Terrasi, F.: Stellar and primordial nucleosynthesis of ^{7}Be: Measurement of ^{3}He$(\alpha, \gamma)^{7}$Be. Phys. Rev. Lett. **102**, 232502 (2009). https://doi.org/10.1103/PhysRevLett.102.232502

[35] Neff, T.: Microscopic calculation of the ^{3}He$(\alpha, \gamma)^{7}$Be and ^{3}H$(\alpha, \gamma)^{7}$Li capture cross sections using realistic interactions. Phys. Rev. Lett. **106**, 042502 (2011). https://doi.org/10.1103/PhysRevLett.106.042502

[36] Dohet-Eraly, J., Navretil, P., Quaglioni, S., Horiuchi, W., Hupin, G., Raimondi, F.: ^{3}He$(\alpha,\gamma)^{7}$Be and ^{3}H$(\alpha,\gamma)^{7}$Li astrophysical S factors from the no-core shell model with continuum". Phys. Lett. B **757**, 430–436 (2016). https://doi.org/10.1016/j.physletb.2016.04.021

[37] Brune, C.R., Kavanagh, R.W., Rolfs, C.: ^{3}H$(\alpha,\gamma)^{7}$Li reaction at low energies. Phys. Rev. C **50**, 2205–2218 (1994). https://doi.org/10.1103/PhysRevC.50.2205

[38] Vogt, K., Mohr, P., Babilon, M., Bayer, W., Galaviz, D., Hartmann, T., Hutter, C., Rauscher, T., Sonnabend, K., Volz, S., Zilges, A.: Measurement of the (γ,n) cross section of the nucleus 197Au close above the reaction threshold. Nucl. Phys. A **707**(1), 241–252 (2002). https://doi.org/10.1016/S0375-9474(02)00922-3

[39] Itoh, O., Utsunomiya, H., Akimune, H., Kondo, T., Kamata, M., Yamagata, T., Toyokawa, H., Harada, H., Kitatani, F., Goko, S., Nair, C., Lui, Y.-W.: Photoneutron Cross Sections for Au Revisited: Measurements with Laser Compton Scattering γ-Rays and Data Reduction by a Least-Squares Method. J. Nucl. Sci. Technol. **48**(5), 834–840 (2011)

[40] Azuma, R.E., Uberseder, E., Simpson, E.C., Brune, C.R., Costantini, H., de Boer, R.J., Görres, J., Heil, M., LeBlanc, P.J., Ugalde, C., Wiescher, M.: AZURE: An R-matrix code for nuclear astrophysics. Phys. Rev. C **81**(4), 045805 (2010). https://doi.org/10.1103/PhysRevC.81.045805

[41] Uberseder, E., deBoer, R.J.: AZURE2 Users Manual (2015). azure.nd.edu

[42] Dormard, J.-J., Assié, M., Grassi, L., Rauly, E., Beaumel, D., Brulin, G., Chabot, M., Coacolo, J.-L., Flavigny, F., Genolini, B., Hammache, F., Barkach, T.I., Rindel, E., Rosier, P., de Séréville, N., Wanlin, E.: Pulse shape discrimination for GRIT: Beam test of a new integrated charge and current preamplifier coupled with high granularity silicon detectors. Nuclear Instruments and Methods in Physics Research Section A: Accelerators, Spectrometers, Detectors and Associated Equipment **1013**, 165641 (2021). https://doi.org/10.1016/j.nima.2021.165641

[43] Labiche, M., Catford, W.N., Lemmon, R.C., Timis, C.N., Chapman, R., Orr, N.A., Fernández-Domínguez, B., Moores, G., Achouri, N.L., Amzal, N., Appleton, S., Ashwood, N.I., Baldwin, T.D., Burns, M., Caballero, L., Cacitti, J., Casadjian, J.M., Chartier, M., Curtis, N., Faiz, K., de France, G., Freer, M., Gautier, J.M., Gelletly, W., Iltis, G., Lecornu, B., Liang, X., Marry, C., Merrer, Y., Olivier, L., Pain, S.D., Pucknell, V.F.E., Raine, B., Rejmund, M., Rubio, B., Saillant, F., Savajols, H., Sorlin, O., Spohr, K., Theisen, C., Voltolini, G., Warner, D.D.: TIARA: A large solid angle silicon array for direct reaction studies with radioactive beams. Nuclear Instruments and Methods in Physics Research Section A: Accelerators, Spectrometers, Detectors and Associated Equipment **614**(3), 439–448 (2010). https://doi.org/10.1016/j.nima.2010.01.009

[44] Bildstein, V., Gernhäuser, R., Kröll, T., Krücken, R., Raabe, R., Duppen, P.V.: A new setup for transfer reactions at REX-ISOLDE. Progress in Particle and Nuclear Physics **59**(1), 386–388 (2007). https://doi.org/10.1016/j.ppnp.2007.01.010

[45] Berner, C., Werner, L., Gernhäuser, R., Kröll, T.: HI-TREX — A highly integrated transfer setup at REX-(HIE)ISOLDE. Nuclear Instruments and Methods in Physics Research Section A: Accelerators, Spectrometers, Detectors and Associated Equipment **987**, 164827 (2021). https://doi.org/10.1016/j.nima.2020.164827

[46] Diget, C.A., Fox, S.P., Smith, A., Williams, S., Porter-Peden, M., Achouri,

L., Adsley, P., Al-Falou, H., Austin, R.A.E., Ball, G.C., Blackmon, J.C., Brown, S., Catford, W.N., Chen, A.A., Chen, J., Churchman, R.M., Dech, J., Valentino, D.D., Djongolov, M., Fulton, B.R., Garnsworthy, A., Hackman, G., Hager, U., Kshetri, R., Kurchaninov, L., Laird, A.M., Martin, J.-P., Matos, M., Orce, J.N., Orr, N.A., Pearson, C.J., Ruiz, C., Sarazin, F., Sjue, S., Smalley, D., Svensson, C.E., Taggart, M., Tardiff, E., Wilson, G.L.: SHARC: Silicon Highly-segmented Array for Reactions and Coulex used in conjunction with the TIGRESS γ-ray spectrometer. Journal of Instrumentation **6**(02), 02005 (2011). https://doi.org/10.1088/1748-0221/6/02/P02005

[47] Pain, S.D., Ratkiewicz, A., Baugher, T., Febbraro, M., Lepailleur, A., Ayangeakaa, A.D., Allen, J., Anderson, J.T., Bardayan, D.W., Blackmon, J.C., Blanchard, R., Burcher, S., Carpenter, M.P., Cha, S.M., Chae, K.Y., Chipps, K.A., Cizewski, J.A., Engelhardt, A., Garland, H., Jones, K.L., Kozub, R.L., Lee, E.J., Hall, M.R., Hall, O., Hu, J., O'Malley, P.D., Marsh, I., Rasco, B.C., Santiago-Gonzales, D., Seweryniak, D., Shadrick, S., Sims, H., Smith, K., Smith, M.S., Tai, P.-L., Thompson, P., Thornsberry, C., Varner, R.L., Walter, D., Wilson, G.L., Zhu, S.: Direct reaction measurements using GODDESS. Physics Procedia **90**, 455–462 (2017). https://doi.org/10.1016/j.phpro.2017.09.051

[48] Ur, C.A., Zilges, A., Pietralla, N., Beller, J., Boisdeffre, B., Cernaianu, M.O., Derya, V., Loher, B., Matei, C., Pascovici, G., Petcu, C., Romig, C., Savran, D., Suliman, G., Udup, E., Werner, V.: Nuclear Resonance Fluorescence Experiments at ELI-NP. Rom. Rep. Phys. **68**, 483–538 (2016)

[49] Söderström, P.-A., Açıksöz, E., Balabanski, D.L., Camera, F., Capponi, L., Ciocan, G., Cuciuc, M., Filipescu, D.M., Gheorghe, I., Glodariu, T., Kaur, J., Krzysiek, M., Matei, C., Roman, T., Rotaru, A., Şerban, A.B., State, A., Utsunomiya, H., Vasilca, V.: ELIGANT-GN — ELI Gamma Above Neutron Threshold: The Gamma-Neutron setup. Nuclear Instruments and Methods in Physics Research Section A: Accelerators, Spectrometers, Detectors and Associated Equipment **1027**, 166171 (2022). https://doi.org/10.1016/j.nima.2021.166171

[50] Heffner, M., Asner, D.M., Baker, R.G., Baker, J., Barrett, S., Brune, C., Bundgaard, J., Burgett, E., Carter, D., Cunningham, M., Deaven, J., Duke, D.L., Greife, U., Grimes, S., Hager, U., Hertel, N., Hill, T., Isenhower, D., Jewell, K., King, J., Klay, J.L., Kleinrath, V., Kornilov, N., Kudo, R., Laptev, A.B., Leonard, M., Loveland, W., Massey, T.N., McGrath, C., Meharchand, R., Montoya, L., Pickle, N., Qu, H., Riot, V., Ruz, J., Sangiorgio, S., Seilhan, B., Sharma, S., Snyder, L., Stave, S., Tatishvili, G., Thornton, R.T., Tovesson, F., Towell, D., Towell, R.S., Watson, S., Wendt, B., Wood, L., Yao, L.: A time projection chamber for

high accuracy and precision fission cross-section measurements. Nuclear Instruments and Methods in Physics Research Section A: Accelerators, Spectrometers, Detectors and Associated Equipment **759**, 50–64 (2014). https://doi.org/10.1016/j.nima.2014.05.057

[51] Koshchiy, E., Rogachev, G.V., Pollacco, E., Ahn, S., Uberseder, E., Hooker, J., Bishop, J., Aboud, E., Barbui, M., Goldberg, V.Z., Hunt, C., Jayatissa, H., Magana, C., O'Dwyer, R., Roeder, B.T., Saastamoinen, A., Upadhyayula, S.: Texas Active Target (TexAT) detector for experiments with rare isotope beams. Nuclear Instruments and Methods in Physics Research Section A: Accelerators, Spectrometers, Detectors and Associated Equipment **957**, 163398 (2020). https://doi.org/10.1016/j.nima.2020.163398

[52] Bishop, J., Parker, C.E., Rogachev, G.V., Ahn, S., Koshchiy, E., Brandenburg, K., Brune, C.R., Charity, R.J., Derkin, J., Dronchi, N., Hamad, G., Jones-Alberty, Y., Kokalova, T., Massey, T.N., Meisel, Z., Ohstrom, E.V., Paneru, S.N., Pollacco, E.C., Saxena, M., Singh, N., Smith, R., Sobotka, L.G., Soltesz, D., Subedi, S.K., Voinov, A.V., Warren, J., Wheldon, C.: Neutron-upscattering enhancement of the triple-alpha process. Nature Communications **13**, 2151 (2022). https://doi.org/10.1038/s41467-022-29848-7

[53] Greisen, K.: End to the Cosmic-Ray Spectrum? Phys. Rev. Lett. **16**, 748–750 (1966). https://doi.org/10.1103/PhysRevLett.16.748

[54] Zatsepin, G.T., Kuz'min, V.A.: Upper limit of the spectrum of cosmic rays. Soviet Journal of Experimental and Theoretical Physics Letters **4**, 78 (1966)

[55] Ohgaki, H., Sugiyama, S., Yamazaki, T., Mikado, T., Chiwaki, M., Yamada, K., Suzuki, R., Noguchi, T., Tomimasu, T.: Measurement of laser-induced Compton backscattered photons with anti-Compton spectrometer. IEEE Transactions on Nuclear Science **38**(2), 386–392 (1991). https://doi.org/10.1109/23.289330

[56] Kii, T., Shima, T., Baba, T., Nagai, Y.: A time projection chamber for the study of nuclear photodisintegration. Nuclear Instruments and Methods in Physics Research Section A: Accelerators, Spectrometers, Detectors and Associated Equipment **552**(3), 329–343 (2005). https://doi.org/10.1016/j.nima.2005.07.003

[57] Shima, T., Nagai, Y., Miyamoto, S., Amano, S., Horikawa, K., Mochizuki, T., Utsunomiya, H., Akimune, H.: Experimental study of nuclear astrophysics with photon beams. AIP Conference Proceedings **1235**(1), 315–321 (2010). https://doi.org/10.1063/1.3442615

[58] Fetisov, V.N., Gorbunov, A.N., Varfolomeev, A.T.: Nuclear photoeffect on three-particle nuclei. Nuclear Physics **71**(2), 305–342 (1965). https://doi.org/10.1016/0029-5582(65)90720-0

[59] Dyer, P., Barnes, C.A.: The $^{12}C(\alpha,\gamma)^{16}O$ reaction and stellar helium burning. Nuclear Physics A **233**(2), 495–520 (1974). https://doi.org/10.1016/0375-9474(74)90470-9

[60] Redder, A., Becker, H.W., Rolfs, C., Trautvetter, H.P., Donoghue, T.R., Rinckel, T.C., Hammer, J.W., Langanke, K.: The $^{12}C(\alpha,\gamma)^{16}O$ cross section at stellar energies. Nuclear Physics A **462**(2), 385–412 (1987). https://doi.org/10.1016/0375-9474(87)90555-0

[61] Ouellet, J.M.L., Butler, M.N., Evans, H.C., Lee, H.W., Leslie, J.R., MacArthur, J.D., McLatchie, W., Mak, H.-B., Skensved, P., Whitton, J.L., Zhao, X., Alexander, T.K.: $^{12}C(\alpha,\gamma)^{16}O$ cross sections at stellar energies. Phys. Rev. C **54**, 1982–1998 (1996). https://doi.org/10.1103/PhysRevC.54.1982

[62] Kunz, R., Jaeger, M., Mayer, A., Hammer, J.W., Staudt, G., Harissopulos, S., Paradellis, T.: $^{12}C(\alpha,\gamma)^{16}O$: The key reaction in stellar nucleosynthesis. Phys. Rev. Lett. **86**, 3244–3247 (2001). https://doi.org/10.1103/PhysRevLett.86.3244

[63] Assunção, M., Fey, M., Lefebvre-Schuhl, A., Kiener, J., Tatischeff, V., Hammer, J.W., Beck, C., Boukari-Pelissie, C., Coc, A., Correia, J.J., Courtin, S., Fleurot, F., Galanopoulos, E., Grama, C., Haas, F., Hammache, F., Hannachi, F., Harissopulos, S., Korichi, A., Kunz, R., LeDu, D., Lopez-Martens, A., Malcherek, D., Meunier, R., Paradellis, T., Rousseau, M., Rowley, N., Staudt, G., Szilner, S., Thibaud, J.P., Weil, J.L.: $E1$ and $E2$ S factors of $^{12}C(\alpha,\gamma_0)^{16}O$ from γ-ray angular distributions with a 4 π-detector array. Phys. Rev. C **73**, 055801 (2006). https://doi.org/10.1103/PhysRevC.73.055801

[64] Schürmann, D., Di Leva, A., Gialanella, L., Kunz, R., Strieder, F., De Cesare, N., De Cesare, M., D'Onofrio, A., Fortak, K., Imbriani, G., Rogalla, D., Romano, M., Terrasi, F.: Study of the 6.05 MeV cascade transition in $^{12}C(\alpha,\gamma)^{16}O$. Physics Letters B **703**(5), 557–561 (2011). https://doi.org/10.1016/j.physletb.2011.08.061

[65] Makii, H., Nagai, Y., Shima, T., Segawa, M., Mishima, K., Ueda, H., Igashira, M., Ohsaki, T.: $E1$ and $E2$ cross sections of the $^{12}C(\alpha,\gamma_0)^{16}O$ reaction using pulsed α beams. Phys. Rev. C **80**, 065802 (2009). https://doi.org/10.1103/PhysRevC.80.065802

[66] Plag, R., Reifarth, R., Heil, M., Käppeler, F., Rupp, G., Voss, F., Wisshak, K.: $^{12}C(\alpha,\gamma)^{16}O$ studied with the Karlsruhe 4π BaF_2 detector. Phys. Rev.

C **86**, 015805 (2012). https://doi.org/10.1103/PhysRevC.86.015805

[67] Barker, F.C., Kajino, T.: The $^{12}C(\alpha,\gamma)^{16}O$ cross section at low energies. Aust. J. Phys. **44**, 369–396 (1991). https://doi.org/10.1071/PH910369

[68] Tischhauser, P., Couture, A., Detwiler, R., Görres, J., Ugalde, C., Stech, E., Wiescher, M., Heil, M., Käppeler, F., Azuma, R.E., Buchmann, L.: Measurement of elastic $^{12}C + \alpha$ scattering: Details of the experiment, analysis, and discussion of phase shifts. Phys. Rev. C **79**, 055803 (2009). https://doi.org/10.1103/PhysRevC.79.055803

[69] Knutson, L.D.: Watson's theorem for low-energy $p - d$ radiative capture. Phys. Rev. C **59**, 2152–2161 (1999). https://doi.org/10.1103/PhysRevC.59.2152

[70] Brune, C.R.: Electric-multipole interference effects in the $^{12}C(\alpha,\gamma_0)^{16}O$ reaction. Phys. Rev. C **64**, 055803 (2001). https://doi.org/10.1103/PhysRevC.64.055803

[71] Gai, M.: Ambiguities in the rate of oxygen formation during stellar helium burning in the $^{12}C(\alpha,\gamma)$ reaction. Phys. Rev. C **88**, 062801 (2013). https://doi.org/10.1103/PhysRevC.88.062801

[72] Brune, C.R., Sayre, D.B.: Energy deconvolution of cross-section measurements with an application to the $^{12}C(\alpha,\gamma)^{16}O$ reaction. Nuclear Instruments and Methods in Physics Research Section A: Accelerators, Spectrometers, Detectors and Associated Equipment **698**, 49–59 (2013). https://doi.org/10.1016/j.nima.2012.09.023

[73] Plaga, R., Becker, H., Redder, A., Rolfs, C., Trautvetter, H., Langanke, K.: The scattering of alpha particles from ^{12}C and the $^{12}C(\alpha,\gamma)^{16}O$ stellar reaction rate. Nuclear Physics A **465**(2), 291–316 (1987). https://doi.org/10.1016/0375-9474(87)90436-2

[74] Bruno, M., Massa, I., Uguzzoni, A., Vannini, G., Verondini, E., Vitale, A.: Experimental study of the α-^{12}C elastic scattering. R-matrix analysis of the phase shifts and ^{16}O levels. Il Nuovo Cimento A (1965-1970) **27**(1), 1–26 (1975). https://doi.org/10.1007/BF02785263

[75] Smith, R., Gai, M., Stern, S., Schweitzer, D., Ahmed, M.: Precision measurements on oxygen formation in stellar helium burning with gamma-ray beams and a Time Projection Chamber. Nature Communications **12**(1), 1–8 (2021). https://doi.org/10.1038/s41467-021-26179-x

[76] Fey, M.: Im Brennpunkt der Nuklearen Astrophysik: Die Reaktion $^{12}C(\alpha,\gamma)^{16}O$. PhD thesis, Universität Stuttgart (2004). https://doi.org/10.18419/opus-4716

[77] deBoer, R.J., Görres, J., Wiescher, M., Azuma, R.E., Best, A., Brune, C.R., Fields, C.E., Jones, S., Pignatari, M., Sayre, D., Smith, K., Timmes, F.X., Uberseder, E.: The $^{12}C(\alpha,\gamma)^{16}O$ reaction and its implications for stellar helium burning. Rev. Mod. Phys. **89**, 035007 (2017). https://doi.org/10.1103/RevModPhys.89.035007

[78] Gai, M., Ahmed, M.W., Stave, S.C., Zimmerman, W.R., Breskin, A., Bromberger, B., Chechik, R., Dangendorf, V., Delbar, T., III, R.H.F., Henshaw, S.S., Kading, T.J., Martel, P.P., McDonald, J.E.R., Seo, P.-N., Tittelmeier, K., Weller, H.R., Young, A.H.: An optical readout TPC (O-TPC) for studies in nuclear astrophysics with gamma-ray beams at HIγS. Journal of Instrumentation **5**(12), 12004 (2010). https://doi.org/10.1088/1748-0221/5/12/P12004

[79] Cwiok, M., Bieda, M., Bihalowicz, J., Dominik, W., Janas, W., Janiak, L., Mańczak, J., Matulewicz, T., Mazzocchi, C., Pfützner, M., *et al.*: A TPC detector for studying photo-nuclear reactions at astrophysical energies with gamma-ray beams at ELI–NP. Acta Phys. Pol. B **49**, 509–514 (2018). https://doi.org/10.5506/APhysPolB.49.509

[80] Gai, M., Schweitzer, D., Stern, S.R., Young, A.H., Smith, R., Cwiok, M., Bihalowicz, J.S., Czyrkowski, H., Dabrowski, R., Dominik, W., Fijalkowska, A., Janas, Z., Janiak, L., Korgul, A., Matulewicz, T., Mazzocchi, C., Pfützner, M., Zaremba, M., Balabanski, D., Gheorghe, I., Matei, C., Tesileanu, O., Zamfir, N.V., Ahmed, M.W., Henshaw, S.S., Howell, C.R., Mueller, J.M., Myers, L.S., Stave, S., Sun, C., Weller, H.R., Wu, Y.K., Breskin, A., Dangendorf, V., Tittelmeier, K., Freer, M.: Time Projection Chamber (TPC) detectors for nuclear astrophysics studies with gamma beams. Nuclear Instruments and Methods in Physics Research Section A: Accelerators, Spectrometers, Detectors and Associated Equipment **954**, 161779 (2020). https://doi.org/10.1016/j.nima.2019.01.006

[81] Cwiok, M., Dominik, W., Fijalkowska, A., Fila, M., Janas, Z., Kalinowski, A., Kierzkowski, K., Kuich, M., Mazzocchi, C., Okli´nski, W., Zaremba, M., Gai, M., Schweitzer, D. K., Stern, S. R., Finch, S., Friman-Gayer, U., Johnson, S. R., Kowalewski, T. M., Balabanski, D. L., Matei, C., Rotaru, A., Haverson, K. C.Z., Smith, R., Allen, R. A.M., Griffiths, M. R., Pirrie, S., Santa Rita Alcibia, P.: Studies of photo-nuclear reactions at astrophysical energies with an active-target tpc. EPJ Web Conf. **279**, 04002 (2023). https://doi.org/10.1051/epjconf/202327904002

[82] Pollacco, E.C., Grinyer, G.F., Abu-Nimeh, F., Ahn, T., Anvar, S., Arokiaraj, A., Ayyad, Y., Baba, H., Babo, M., Baron, P., Bazin, D., Beceiro-Novo, S., Belkhiria, C., Blaizot, M., Blank, B., Bradt, J., Cardella, G., Carpenter, L., Ceruti, S., De Filippo, E., Delagnes, E., De Luca, S.,

De Witte, H., Druillole, F., Duclos, B., Favela, F., Fritsch, A., Giovinazzo, J., Gueye, C., Isobe, T., Hellmuth, P., Huss, C., Lachacinski, B., Laffoley, A.T., Lebertre, G., Legeard, L., Lynch, W.G., Marchi, T., Martina, L., Maugeais, C., Mittig, W., Nalpas, L., Pagano, E.V., Pancin, J., Poleshchuk, O., Pedroza, J.L., Pibernat, J., Primault, S., Raabe, R., Raine, B., Rebii, A., Renaud, M., Roger, T., Roussel-Chomaz, P., Russotto, P., Saccà, G., Saillant, F., Sizun, P., Suzuki, D., Swartz, J.A., Tizon, A., Trifiró, A., Usher, N., Wittwer, G., Yang, J.C.: Get: A generic electronics system for TPCs and nuclear physics instrumentation. Nuclear Instruments and Methods in Physics Research Section A: Accelerators, Spectrometers, Detectors and Associated Equipment **887**, 81–93 (2018). https://doi.org/10.1016/j.nima.2018.01.020

[83] Preliminary report for experiment HIGS P-14-21/P-18-19. Technical report, Warsaw TPC collaboration (2021)